

# $W_H$ -pair Production in the Littlest Higgs Model with $T$ parity in next-to-leading order QCD at LHC

Du Song-Ming, Guo Lei, Liu Wen, Ma Wen-Gan, and Zhang Ren-You  
Department of Modern Physics, University of Science and Technology  
of China (USTC), Hefei, Anhui 230026, P.R.China

## Abstract

In the framework of the littlest Higgs model with  $T$  parity, we study the  $W_H$ -pair production at the CERN Large Hadron Collider up to the QCD next-to-leading order (NLO). The kinematic distributions of final decay products and the theoretical dependence of the cross section on the factorization/renormalization scale are analyzed. We adopt the PROSPINO scheme in the QCD NLO calculations to avoid double counting and keep the convergence of the perturbative QCD description. Our numerical results show that the QCD NLO corrections significantly reduce the scale uncertainty, and enhance the leading order integrated cross section with a  $K$ -factor in the range of 1.10 – 1.22 (1.09 – 1.17) with the symmetry breaking scale  $f$  varying from 400  $GeV$  (400  $GeV$ ) to 1.5  $TeV$  (1.0  $TeV$ ) at the 14  $TeV$  (8  $TeV$ ) LHC. We find that it is possible to select the signal events of the  $W_H$ -pair production from the  $pp \rightarrow W^+W^- \rightarrow e^+\mu^-\nu_e\bar{\nu}_\mu + X$  background with high ratio of signature over background by taking proper lower limits on transverse momenta, invariant mass of the final charged leptons and the missing transverse momentum.

PACS: 12.38.Bx, 12.60.Cn, 14.70.Pw

## I. Introduction

Although the standard model (SM) [1, 2] provides a remarkably successful description of high energy physics phenomena at the energy scale up to  $100 \text{ GeV}$ , it leaves a number of theoretical problems unsolved. Many extended models are proposed to deal with these problems such as grand unified theories [3], supersymmetric models [4], extra dimensions models [5], left-right symmetric models [6], B-L (baryon number minus lepton number) extended SM models [7], little Higgs models [8] and many more. Each of these models has motivation to solve one or more of the problems that the SM encounters. Among them the little Higgs models deserve attention due to their elegant solution to hierarchy problem and are proposed as one kind of electroweak symmetry breaking (EWSB) models without fine-tuning in which the Higgs boson is naturally light as a result of nonlinearly realized symmetry [9]-[14]. The lightest Higgs (LH) model [15], an  $SU(5)/SO(5)$  nonlinear sigma model [11], is the most simplest version of little Higgs models, in which a set of new heavy gauge bosons ( $A_H, W_H, Z_H$ ) and a vector-like quark ( $T$ ) are introduced to cancel the quadratic divergence contribution to Higgs boson mass from the SM gauge boson loops and the top quark loop respectively. However, this model predicts large corrections to electroweak precision observables and the scale of the global symmetry breaking  $f$ , is constrained by experimental data [12], which set severe constraints on the new heavy particle masses and the model parameters. For instance, recent experimental measurements on the decay processes of  $W_H^\mp \rightarrow l^\mp \bar{\nu}^{(-)}$  and  $Z_H \rightarrow l^+l^-$  provide the constraints of  $M_{W_H} > 2.18 \text{ TeV}$  and  $M_{Z_H} > 1.83 \text{ TeV}$  [16, 17]. These constraints would enforce the symmetry breaking scale  $f$ , which characterizes the mass of new particles, to be larger than  $2.5 \text{ TeV}$  and  $3 \text{ TeV}$  respectively. Consequently, the cutoff scale  $\Lambda \sim 4\pi f$  becomes so large that calls for the fine-tuning between the electroweak scale and the cutoff scale again.

By introducing a discrete symmetry, the  $T$  parity, the lightest Higgs model with  $T$  parity (LHT) [18]-[22] offers a viable solution to the naturalness problem of the SM, and also predicts a set of new heavy fermions, gauge bosons as well as a candidate for dark matter. In the LHT, all the SM particles are  $T$ -even and almost all the new heavy particles are  $T$ -odd. Due to the different  $T$  parity quantum numbers, the SM gauge bosons cannot mix with the new gauge bosons in the LHT. This would alleviate the constraints from the electroweak precision tests and thus allows the scale  $f$  to

be significantly lower than 1  $TeV$  [21]. For instance, due to the  $T$  parity conservation, the processes  $W_H^\mp \rightarrow l^\mp \begin{pmatrix} \nu \\ \nu \end{pmatrix}$  and  $Z_H \rightarrow l^+l^-$  are forbidden, and the only decay modes of these  $T$ -odd heavy gauge bosons are  $W_H \rightarrow A_H W$  and  $Z_H \rightarrow A_H H$ . In this case, the leptons are produced from the decays of  $W$  and  $H$ , but not from the heavy gauge bosons directly. Therefore, these  $T$ -even gauge bosons escape from the experimental constraints shown in Refs.[16, 17]. Furthermore, as a lightest  $T$ -odd particle, the heavy photon  $A_H$  cannot further decay into other particles, and would be a good candidate for the dark matter [23]. Since the CERN Large Hadron Collider (LHC) has potential to detect the signals of new gauge bosons and fermions, the phenomenology of the LHT would be quite interesting and a number of phenomenological works has been presented [20, 24, 25, 26]. Recently, the QCD NLO corrections to the process  $pp \rightarrow W_H(Z_H)q_- + X$  has been presented in Ref.[27]. Of all heavy gauge boson production processes, the heavy gauge boson  $W_H$ -pair production can be particularly significant due to the potential of its copious productions at the LHC as shown in Refs.[24, 28], where the  $W_H$ -pair production at the LHC is studied at the leading-order (LO).

In this paper, we make a precision investigation for the process  $pp \rightarrow W_H^+ W_H^- + X$  at the LHC including the QCD NLO corrections. In Sec.II we make a brief review of the relevant theory of the LHT. The detailed strategies of the calculation are given in Sec.III. The numerical results and discussions are presented in Sec.IV. Finally we present a short summary.

## II. The related LHT theory

Before our calculations, we will briefly recapitulate the LHT theory which is relevant to the analysis in this work. The details of the LHT can be found in Refs.[18, 20, 21, 24].

At some high scale  $f$  the global symmetry  $SU(5)$  is broken down to  $SO(5)$ , leading to 14 massless Nambu-Goldstone bosons. Four of them are manifested as the longitudinal modes of the heavy gauge bosons. The other 10 decompose into a  $T$ -even  $SU(2)$  doublet  $h$ , identified as the SM Higgs field, and a complex  $T$ -odd  $SU(2)$  triplet  $\Phi$ , which obtains a mass of  $m_\Phi = \sqrt{2}m_h f/v_{SM}$ , with  $m_h$  and  $v_{SM}$  being SM Higgs mass and the electroweak symmetry break scale, respectively.

The additional discrete symmetry,  $T$ -parity, is in analogy to the  $R$ -parity in the minimal supersymmetric standard model (MSSM) [18, 20, 22]. The  $T$ -parity transformations for gauge sector are defined as the exchange between the gauge bosons of the two  $SU(2) \times U(1)$  groups, i.e.,  $W_1^a \leftrightarrow W_2^a$

and  $B_1 \leftrightarrow B_2$ . Thus their  $T$ -odd and  $T$ -even combinations can be obtained as

$$\begin{aligned} W_H^a &= \frac{1}{\sqrt{2}}(W_1^a - W_2^a), & B_H &= \frac{1}{\sqrt{2}}(B_1 - B_2), & (T - \text{odd}), \\ W_L^a &= \frac{1}{\sqrt{2}}(W_1^a + W_2^a), & B_L &= \frac{1}{\sqrt{2}}(B_1 + B_2), & (T - \text{even}). \end{aligned} \quad (2.1)$$

The mass eigenstates of the gauge sector in the LHT are expressed as

$$\begin{aligned} W_H^\pm &= \frac{1}{\sqrt{2}}(W_H^1 \mp iW_H^2), & Z_H &= s_H B_H + c_H W_H^3, & A_H &= c_H B_H - s_H W_H^3, \\ W_L^\pm &= \frac{1}{\sqrt{2}}(W_L^1 \mp iW_L^2), & Z_L &= -s_w B_L + c_w W_L^3, & A_L &= c_w B_L + s_w W_L^3, \end{aligned} \quad (2.2)$$

where  $s_w = \sin \theta_W$ ,  $c_w = \cos \theta_W$ ,  $s_H = \sin \theta_H$ ,  $c_H = \cos \theta_H$ ,  $\theta_W$  is the Weinberg angle, and the mixing angle  $\theta_H$  at the  $\mathcal{O}(v^2/f^2)$  is expressed as

$$\sin \theta_H \simeq \left[ \frac{5gg'}{4(5g^2 - g'^2)} \frac{v_{SM}^2}{f^2} \right]. \quad (2.3)$$

Then the gauge sector consists of  $T$ -odd heavy new gauge bosons  $W_H^\pm$ ,  $Z_H$ ,  $A_H$  and  $T$ -even light gauge bosons identified as SM gauge bosons,  $W^\pm$ ,  $Z^0$  and one massless photon. The  $T$  parity partner of the photon,  $A_H$ , is the lightest  $T$ -odd particle, therefore, the candidate of dark matter in the LHT. The masses of the  $T$  parity partners of the photon,  $Z^0$ - and  $W^\pm$ -boson are expressed as [24]

$$m_{W_H} \simeq m_{Z_H} \simeq gf \left( 1 - \frac{1}{8} \frac{v_{SM}^2}{f^2} \right), \quad m_{A_H} \simeq \frac{1}{\sqrt{5}} g' f \left( 1 - \frac{5}{8} \frac{v_{SM}^2}{f^2} \right), \quad (2.4)$$

where  $v_{SM} = 246 \text{ GeV}$ . At the tree level the SM gauge boson masses can be expressed as  $m_W = \frac{gv_{SM}}{2}$  and  $m_Z = \frac{v_{SM}\sqrt{g^2+g'^2}}{2}$ .

In the LHT, the fermion sector of the first two generations in the SM is remained unchanged and the third generation of quarks is modified. We introduce two fermion doublets  $q_1$  and  $q_2$  for each fermion generation. The  $T$  parity transformation to these fermion doublets is defined as  $q_1 \leftrightarrow -q_2$ . Therefore, the  $T$ -odd and  $T$ -even combinations can be constructed as  $q_- = \frac{1}{\sqrt{2}}(q_1 + q_2)$  and  $q_+ = \frac{1}{\sqrt{2}}(q_1 - q_2)$ , where  $q_+$  is the doublet for the SM fermions and  $q_-$  for their  $T$ -odd partners. We take the Lagrangian suggested in Refs.[18, 20, 21] to generate the masses of the  $T$ -odd fermion doublets,

$$- \kappa f (\bar{\Psi}_2 \xi \Psi_c + \bar{\Psi}_1 \Sigma_0 \Omega \xi^\dagger \Omega \Psi_c) + \text{h.c.}, \quad (2.5)$$

where  $\Omega = \text{diag}(1, 1, -1, 1, 1)$ ,  $\Psi_c = (q_c, \chi_c, \tilde{q}_c)^T$ , and the  $SU(5)$  multiplets  $\Psi_1$  and  $\Psi_2$  are expressed as

$$\Psi_1 = \begin{pmatrix} q_1 \\ 0 \\ \mathbf{0}_2 \end{pmatrix}, \quad \Psi_2 = \begin{pmatrix} \mathbf{0}_2 \\ 0 \\ q_2 \end{pmatrix}. \quad (2.6)$$

The interaction Lagrangian in Eq.(2.5) can be proofed to be invariant under  $T$ -parity, and  $T$ -odd quark doublet  $q_-$  gets a Dirac mass with  $\tilde{q}_c \equiv (id_{R_-}, -iu_{R_-})^T$  from Eq.(2.5) expressed as [24]

$$m_{U_-} \simeq \sqrt{2}\kappa f \left(1 - \frac{1}{8} \frac{v_{SM}^2}{f^2}\right), \quad m_{D_-} = \sqrt{2}\kappa f, \quad (2.7)$$

where the lower indexes  $U_- = u_-, c_-, t_-$  and  $D_- = d_-, s_-, b_-$ , which represent the  $T$ -odd heavy partners of the SM quarks, and  $\kappa$  is the mass coefficient in Lagrangian of the quark sector. As we know in the LHT  $f > 500 \text{ GeV}$  [29], it is evident from Eq.(2.7) that the  $T$ -odd up- and down-type heavy partners have nearly equal masses.

In order to avoid the large radiative correction to Higgs boson mass induced by top-quark loop, the top sector must be additionally modified. We introduce the following two multiplets,

$$\mathcal{Q}_1 = \begin{pmatrix} q_1 \\ U_{L1} \\ \mathbf{0}_2 \end{pmatrix}, \quad \mathcal{Q}_2 = \begin{pmatrix} \mathbf{0}_2 \\ U_{L2} \\ q_2 \end{pmatrix}, \quad (2.8)$$

where  $U_{L1}$  and  $U_{L2}$  are the singlet fields and the  $q_1$  and  $q_2$  are the doublets. Under the  $SU(5)$  and the  $T$  parity transformations,  $\mathcal{Q}_1$  and  $\mathcal{Q}_2$  behave themselves same as  $\Psi_1$  and  $\Psi_2$ .

In addition to the  $T$ -even SM top quark right-handed  $SU(2)$  singlet  $u_R$ , the LHT contains two  $SU(2)$  singlet fermions  $U_{R1}$  and  $U_{R2}$  of hypercharge  $2/3$ , which transform under  $T$  parity as

$$U_{R1} \leftrightarrow -U_{R2}. \quad (2.9)$$

The  $T$  parity invariant Yukawa Lagrangian of the top sector can be written as

$$\begin{aligned} \mathcal{L}_t^Y &= \frac{\lambda_1 f}{2\sqrt{2}} \epsilon_{ijk} \epsilon_{xy} [(\bar{\mathcal{Q}}_1)_i \Sigma_{jx} \Sigma_{ky} - (\bar{\mathcal{Q}}_2 \Sigma_0)_i \tilde{\Sigma}_{jx} \tilde{\Sigma}_{ky}] u_R \\ &+ \lambda_2 f (\bar{U}_{L1} U_{R1} + \bar{U}_{L2} U_{R2}) + \text{h.c.} . \end{aligned} \quad (2.10)$$

where  $\tilde{\Sigma} = \Sigma_0 \Omega \Sigma^\dagger \Omega \Sigma_0$  is the image of the  $\Sigma$  field under  $T$  parity, and  $i, j$  and  $k$  run over  $1 - 3$  and  $x$  and  $y$  over  $4 - 5$ . The  $T$  parity eigenstates are constructed as

$$q_\pm = \frac{1}{\sqrt{2}}(q_1 \mp q_2), \quad U_{L\pm} = \frac{1}{\sqrt{2}}(U_{L1} \mp U_{L2}), \quad U_{R\pm} = \frac{1}{\sqrt{2}}(U_{R1} \mp U_{R2}). \quad (2.11)$$

The  $T$ -odd states  $U_{L-}$  and  $U_{R-}$  combine to form a Dirac fermion  $T_-$ , and we obtain the mass of the  $T_-$  quark from the Lagrangian of Eq.(2.10) as

$$m_{T_-} = \lambda_2 f. \quad (2.12)$$

The left-handed (right-handed) top quark  $t$  is a linear combination of  $u_{L+}$  and  $U_{L+}$  ( $u_{R+}$  and  $U_{R+}$ ), and another independent linear combination is a heavy  $T$ -even partner of the top quark  $T_+$ :

$$\begin{pmatrix} t_X \\ T_{+X} \end{pmatrix} = \begin{pmatrix} c_X & -s_X \\ s_X & c_X \end{pmatrix} \begin{pmatrix} u_{X+} \\ U_{X+} \end{pmatrix}, \quad (X = L, R), \quad (2.13)$$

where the mixing matrix elements are approximately expressed as

$$s_L = s_\alpha^2 \frac{v_{SM}}{f} + \dots, \quad s_R = s_\alpha \left[ 1 - \frac{c_\alpha^2 (c_\alpha^2 - s_\alpha^2) v_{SM}^2}{2 f^2} + \dots \right]. \quad (2.14)$$

There we define  $s_\alpha = \lambda_1 / \sqrt{\lambda_1^2 + \lambda_2^2}$  and  $c_\alpha = \lambda_2 / \sqrt{\lambda_1^2 + \lambda_2^2}$ . The  $t$  is identified with the SM top and  $T_+$  is its  $T$ -even heavy partner. Then the masses of the top quark and  $T$ -even heavy top quark can be obtained as

$$m_t \simeq \frac{\lambda_1 \lambda_2 v_{SM}}{\sqrt{\lambda_1^2 + \lambda_2^2}}, \quad m_{T_+} \simeq f \sqrt{\lambda_1^2 + \lambda_2^2}. \quad (2.15)$$

The Feynman rules in the LHT related to our calculations are presented in Appendix A.

### III. Calculation descriptions

In this work, we adopt the five-flavor scheme (5FS) in the LO and QCD NLO calculations and neglect the masses of the  $u, d, c, s, b$  quarks. In our calculations we use the 't Hooft-Feynman gauge and employ developed FeynArts 3.4 package [30] to generate Feynman diagrams and their corresponding amplitudes. The reduction of output amplitudes are implemented by FormCalc-5.4 package [31].

#### III.1 LO cross section

The LO contribution to the cross section for the parent process  $pp \rightarrow W_H^+ W_H^- + X$  comes from the quark-antiquark annihilation. We denote the subprocess as

$$q(p_1) + \bar{q}(p_2) \rightarrow W_H^+(p_3) + W_H^-(p_4), \quad (q = u, d, c, s, b). \quad (3.1)$$

The corresponding Feynman diagrams for the  $u\bar{u} \rightarrow W_H^+ W_H^-$  partonic process are shown in Fig.1, the LO Feynman diagrams for other partonic processes  $q\bar{q} \rightarrow W_H^+ W_H^- (q = d, c, s, b)$  are similar with those

in Fig.1 and are not depicted there. Figs.1(1,2) correspond to the exchanges of  $\gamma$  and  $Z^0$  gauge bosons separately, and the diagram with exchange of a  $T$ -odd quark is shown in Fig.1(3). The amplitudes of the tree-level Feynman diagrams in Figs.1 for the partonic process  $u\bar{u} \rightarrow W_H^+ W_H^-$  are respectively expressed as

$$\begin{aligned}
\mathcal{M}_{u\bar{u}}^{(1)} &= -\frac{2e^2}{3\hat{s}} \bar{v}(p_2) \left[ (\not{p}_3 - \not{p}_4) \epsilon^*(p_3) \cdot \epsilon^*(p_4) - (2p_3 + p_4) \cdot \epsilon^*(p_4) \not{\epsilon}^*(p_3) + (2p_4 + p_3) \cdot \epsilon^*(p_3) \not{\epsilon}^*(p_4) \right] u(p_1), \\
\mathcal{M}_{u\bar{u}}^{(2)} &= -\frac{e^2}{2s_w^2(\hat{s} - m_Z^2)} \bar{v}(p_2) \left[ (\not{p}_3 - \not{p}_4) \epsilon^*(p_3) \cdot \epsilon^*(p_4) - (2p_3 + p_4) \cdot \epsilon^*(p_4) \not{\epsilon}^*(p_3) \right. \\
&\quad \left. + (2p_4 + p_3) \cdot \epsilon^*(p_3) \not{\epsilon}^*(p_4) \right] \cdot \left( P_L - \frac{4}{3}s_w^2 \right) u(p_1), \\
\mathcal{M}_{u\bar{u}}^{(3)} &= -\frac{e^2}{2s_w^2[(p_1 - p_3)^2 - m_{d_-}^2]} \bar{v}(p_2) \not{\epsilon}^*(p_4) P_L \left[ (\not{p}_1 - \not{p}_3) + m_{d_-} \right] \not{\epsilon}^*(p_3) P_L u(p_1), \tag{3.2}
\end{aligned}$$

where  $P_L = \frac{1}{2}(1 - \gamma_5)$ . Analogously, we can get the amplitudes for the other partonic processes  $q\bar{q} \rightarrow W_H^+ W_H^-$  ( $q = d, c, s, b$ ). The LO amplitude for the partonic process  $q\bar{q} \rightarrow W_H^+ W_H^-$  can be generally expressed by summing up all the above three total amplitudes,

$$\mathcal{M}_{q\bar{q}}^{LO} = \sum_{i=1}^3 \mathcal{M}_{q\bar{q}}^{(i)}, \quad (q = u, d, c, s, b). \tag{3.3}$$

The LO cross section for the partonic process  $q\bar{q} \rightarrow W_H^+ W_H^-$  then can be obtained as

$$\hat{\sigma}_{q\bar{q}}^0 = \frac{1}{4} \frac{1}{9} \frac{(2\pi)^4}{4|\vec{p}| \sqrt{\hat{s}}} \int \sum_{spin} \sum_{color} |\mathcal{M}_{q\bar{q}}^{LO}|^2 d\Omega_2, \quad (q = u, d, c, s, b). \tag{3.4}$$

The factor  $\frac{1}{4}$  and  $\frac{1}{9}$  come from averaging over the spins and colors of the initial partons respectively,  $\vec{p}$  is the three-momentum of one initial parton in center-of-mass system (CMS) and  $\sqrt{\hat{s}}$  is the partonic CMS energy. The two-body phase-space element  $d\Omega_2$  is expressed as

$$d\Omega_2 = \delta^{(4)}(p_1 + p_2 - p_3 - p_4) \frac{d^3 \vec{p}_3}{(2\pi)^3 2E_3} \frac{d^3 \vec{p}_4}{(2\pi)^3 2E_4}. \tag{3.5}$$

The total cross section for the parent process  $pp \rightarrow W_H^+ W_H^- + X$  at the tree-level can be obtained by integrating the cross section for partonic processes  $\hat{\sigma}_{q\bar{q}}^0$  with the parton distribution functions (PDFs),

$$\sigma_{LO} = \sum_{q=u,d}^{c,s,b} \int_0^1 dx_1 \int_0^1 dx_2 [G_{q/P_1}(x_1, \mu_f) G_{\bar{q}/P_2}(x_2, \mu_f) + (1 \leftrightarrow 2)] \hat{\sigma}_{q\bar{q}}^0(\hat{s} = x_1 x_2 s), \tag{3.6}$$

where  $G_{i/P}$  ( $i = q, \bar{q}; P = P_1, P_2$ ) denotes the PDF of parton  $i$  in proton  $P$ ,  $x_i$  ( $i = 1, 2$ ) is the momentum fraction of a parton in proton  $P_i$  ( $i = 1, 2$ ),  $\mu_f$  is the factorization scale and  $s$  is the total colliding energy squared in proton-proton CMS.

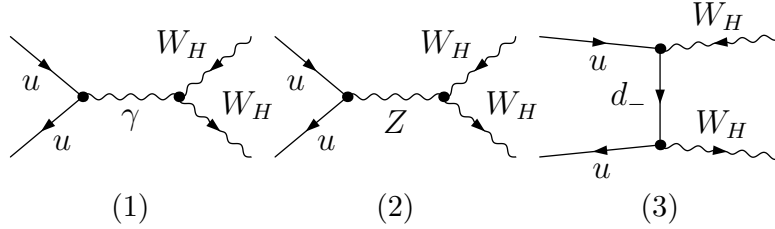


Figure 1: The LO Feynman diagrams for the partonic process  $u\bar{u} \rightarrow W_H^+ W_H^-$ .

### III..2 QCD NLO corrections

The genuine QCD NLO correction to the parent process  $pp \rightarrow W_H^+ W_H^- + X$  includes the following components: (1) The QCD one-loop virtual corrections to the partonic processes  $q\bar{q} \rightarrow W_H^+ W_H^-$ . (2) The contribution of the real gluon emission partonic process  $q\bar{q} \rightarrow W_H^+ W_H^- + g$ . (3) The contribution of the real light-(anti)quark emission partonic process  $q(\bar{q})g \rightarrow W_H^+ W_H^- + q(\bar{q})$ . (4) The corresponding collinear counterterms of the PDFs. In order to isolate the ultraviolet (UV) and infrared (IR) singularities in the NLO calculations, we adopt the dimensional regularization (DR) method in  $D = 4 - 2\epsilon$  dimensions.

#### III..2.1 One-loop corrections to $q\bar{q} \rightarrow W_H^+ W_H^-$ partonic process

We plotted some representative Feynman diagrams for the one-loop virtual corrections to the partonic process  $u\bar{u} \rightarrow W_H^+ W_H^-$  in Fig.2. In calculating one-loop amplitudes we shall meet both UV and IR singularities. In order to remove the UV divergences, we renormalize the masses and wave functions of SM quarks and their  $T$ -odd partners with the counterterms defined as

$$\psi_{q,L,R}^0 = \left(1 + \frac{1}{2}\delta Z_{q,L,R}\right) \psi_{q,L,R}, \quad (3.7)$$

$$\psi_{q-,L,R}^0 = \left(1 + \frac{1}{2}\delta Z_{q-,L,R}\right) \psi_{q-,L,R}, \quad (3.8)$$

$$m_{q-}^0 = m_{q-} + \delta m_{q-}, \quad (3.9)$$

where  $\psi_{q,L,R}, \psi_{q-,L,R}$  denote the fields of SM quark and  $T$ -odd quark respectively, and  $m_{q-}$  denotes the mass of  $T$ -odd quark. We adopt the on-shell scheme to perform the renormalization procedure and then the relevant renormalization constants are expressed as

$$\delta Z_{q,L,R} = -\frac{\alpha_s(\mu_r)}{3\pi} [\Delta_{UV} - \Delta_{IR}], \quad (3.10)$$

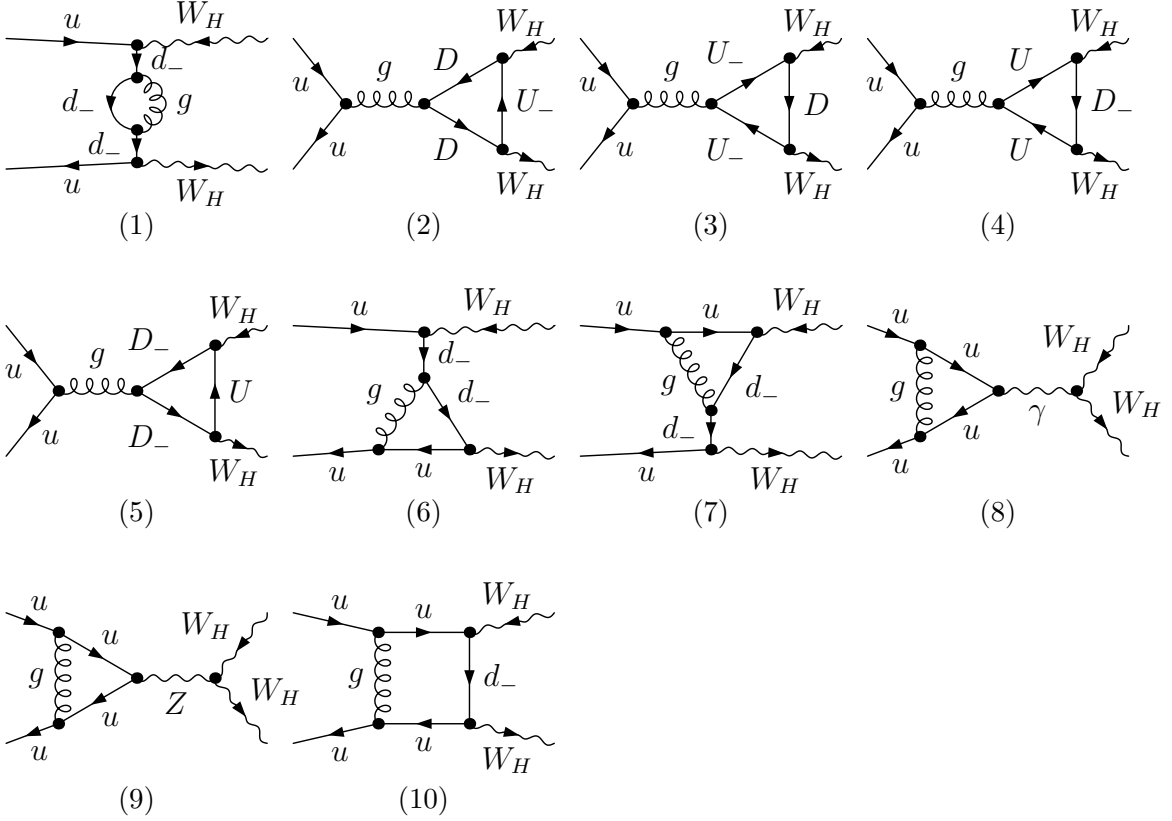


Figure 2: The representative one-loop Feynman diagrams for the partonic process  $u\bar{u} \rightarrow W_H^+ W_H^-$ , where  $(U_-, D) = (u_-, d), (c_-, s), (t_-, b)$  and  $(U, D_-) = (u, d_-), (c, s_-), (t, b_-)$ .

$$\delta Z_{q_-, L, R} = -\frac{\alpha_s(\mu_r)}{3\pi} \left[ \Delta_{UV} + 2\Delta_{IR} + 4 + 3 \ln \left( \frac{\mu_r^2}{m_{q_-}^2} \right) \right], \quad (3.11)$$

$$\frac{\delta m_{q_-}}{m_{q_-}} = -\frac{\alpha_s(\mu_r)}{3\pi} \left\{ 3 \left[ \Delta_{UV} + \ln \left( \frac{\mu_r^2}{m_{q_-}^2} \right) \right] + 4 \right\}, \quad (3.12)$$

where  $\Delta_{UV} = \frac{1}{\epsilon_{UV}} - \gamma_E + \ln(4\pi)$  and  $\Delta_{IR} = \frac{1}{\epsilon_{IR}} - \gamma_E + \ln(4\pi)$ . After the renormalization, this one-loop virtual contribution is UV finite. However, it still contains soft and collinear IR singularities, which can be canceled by considering the real gluon/light-(anti)quark emission subprocesses and the PDF counterterms as described in the following subsections.

### III..2.2 Real gluon/light-(anti)quark emission corrections

We denote the real gluon emission partonic process for the  $W_H$ -pair production as

$$q(p_1) + \bar{q}(p_2) \rightarrow W_H^+(p_3) + W_H^-(p_4) + g(p_5), \quad (q = u, d, c, s, b). \quad (3.13)$$

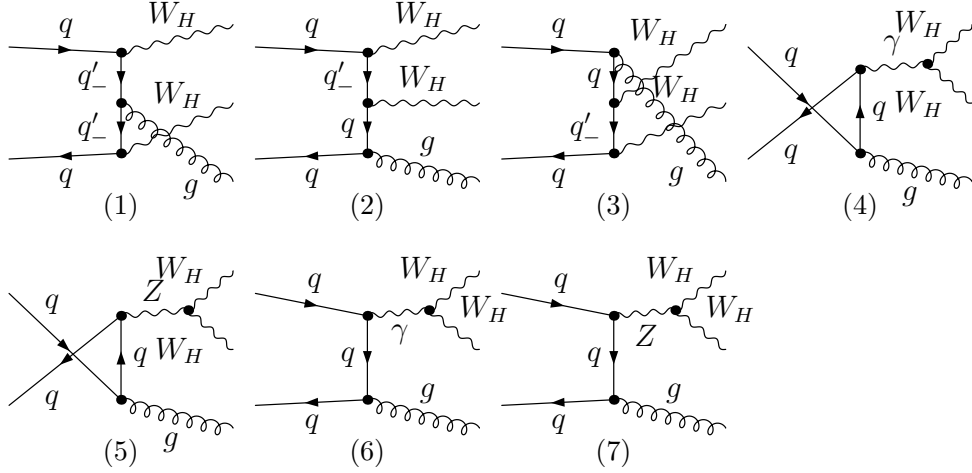


Figure 3: The tree-level Feynman diagrams for the real gluon emission partonic process  $q\bar{q} \rightarrow W_H^+ W_H^- + g$ , ( $q = u, d, c, s, b$ ).

The Feynman diagrams for this subprocess are shown in Fig.3. There exist soft and collinear singularities in these diagrams. In order to manipulate these IR divergences, we employ the two cutoff phase-space slicing (TCPSS) methods [32], which introduce two arbitrary cutoff  $\delta_s$  and  $\delta_c$ . The soft cutoff  $\delta_s$  divides the phase-space into two regions: soft region ( $E_5 \leq \frac{1}{2}\delta_s\sqrt{\hat{s}}$ ) and hard region ( $E_5 > \frac{1}{2}\delta_s\sqrt{\hat{s}}$ ), another cutoff  $\delta_c$  separates the hard region into hard collinear ( $HC$ ) region ( $\hat{s}_{15} \leq \delta_c\hat{s}$  or  $\hat{s}_{25} \leq \delta_c\hat{s}$ ) and hard noncollinear ( $\overline{HC}$ ) region. Then we can express the real gluon emission subprocess cross section as

$$\hat{\sigma}_g = \hat{\sigma}_g^S + \hat{\sigma}_g^{HC} + \hat{\sigma}_g^{\overline{HC}}. \quad (3.14)$$

The noncollinear cross section part  $\hat{\sigma}_g^{\overline{HC}}$  is IR safe and the soft singularity in the soft part  $\hat{\sigma}_g^S$  can be canceled by the soft IR divergence in the virtual corrections, as demonstrated by the Kinoshita-Lee-Nauenberg (KLN) theorem [33]. The collinear singularity can be partially canceled by the virtual corrections, and the remained collinear divergence can be absorbed by the PDF counterterms.

The real light-(anti)quark emission partonic process for the  $W_H$ -pair production is denoted as

$$q/\bar{q}(p_1) + g(p_2) \rightarrow W_H^+(p_3) + W_H^-(p_4) + q/\bar{q}(p_5), \quad (q = u, d, c, s, b). \quad (3.15)$$

We depict the tree-level Feynman diagrams for the real light-quark emission partonic process  $qg \rightarrow W_H^+ W_H^- + q$  in Fig.4. We notice that there could exist resonance effect in Figs.4(3) and (5) due to possible one-shell  $q_-$  propagator. In order to deal with resonance singularity, we replace the  $q_-$  mass

squared  $m_{q_-}^2$  in its propagator by  $m_{q_-}^2 - im_{q_-}\Gamma_{q_-}$ . The expressions for the partial decay widths of T-odd quarks are given in Appendix B. This extremely large correction to Born  $pp \rightarrow W_H^+ W_H^- + X$  process would eventually destroy the perturbative convergence. Furthermore, Figs.4(3) and (5) are included also in the  $W_H q_-$  associated production process followed by an on-shell decay  $q_- \rightarrow W_H q'$ . In order to avoid double counting and to keep the convergence of the perturbative QCD description of the  $pp \rightarrow W_H^+ W_H^- + X$  process, we need to remove the intermediate on-shell T-odd quark  $q_-$  contributions. This removal can be implemented by adopting the PROSPINO subtraction strategy [34, 35], which is done by performing a replacement of the Breit-Wigner propagator:

$$\frac{|\mathcal{M}|^2(s_{W_H q})}{(s_{W_H q} - m_{q_-}^2)^2 + m_{q_-}^2 \Gamma_{q_-}^2} \rightarrow \frac{|\mathcal{M}|^2(s_{W_H q})}{(s_{W_H q} - m_{q_-}^2)^2 + m_{q_-}^2 \Gamma_{q_-}^2} - \frac{|\mathcal{M}|^2(m_{q_-}^2)}{(s_{W_H q} - m_{q_-}^2)^2 + m_{q_-}^2 \Gamma_{q_-}^2} \Theta(\hat{s} - 4m_{q_-}^2) \Theta(m_{q_-} - m_{W_H}), \quad (3.16)$$

where  $s_{W_H q}$  is the squared momentum flowing through the intermediate  $q_-$  propagator. For the real light-(anti)quark emission corrections we use the cutoff  $\delta_c$  to separate the phase-space into collinear ( $C$ ) region ( $\hat{s}_{15} \leq \delta_c \hat{s}$  or  $\hat{s}_{25} \leq \delta_c \hat{s}$ ) and noncollinear ( $\bar{C}$ ) region ( $\hat{s}_{15} > \delta_c \hat{s}$  and  $\hat{s}_{25} > \delta_c \hat{s}$ ). Then we have

$$\hat{\sigma}_{q(\bar{q})} = \hat{\sigma}_{q(\bar{q})}^C + \hat{\sigma}_{q(\bar{q})}^{\bar{C}}, \quad (3.17)$$

where  $\hat{\sigma}_q^{\bar{C}}$  is finite and  $\hat{\sigma}_q^C$  contains collinear singularity. After summing the virtual and real gluon/(anti)quark radiation corrections, the remained collinear divergence can be canceled by that in the NLO PDFs.

### III..2.3 PDF counterterms

As mentioned above, part of the collinear divergences in the virtual corrections to  $q\bar{q} \rightarrow W_H^+ W_H^-$  channel can be canceled by the real gluon/light-(anti)quark emission partonic processes, and the remained collinear divergences are absorbed in the PDF counterterms. This collinear counterterm of the PDF can be denoted as  $\delta G_{i/P}(x, \mu_f)$  ( $P = P_1, P_2$  and  $i = g, u, \bar{u}, d, \bar{d}, c, \bar{c}, s, \bar{s}, b, \bar{b}$ ). We divided  $\delta G_{i/P}(x, \mu_f)$  into two parts: the collinear gluon emission part  $\delta G_{i/P}^{(gluon)}(x, \mu_f)$  and the collinear light-quark emission part  $\delta G_{i/P}^{(quark)}(x, \mu_f)$ ,

$$\delta G_{q(g)/P}(x, \mu_f) = \delta G_{q(g)/P}^{(gluon)}(x, \mu_f) + \delta G_{q(g)/P}^{(quark)}(x, \mu_f),$$

$$(q = u, \bar{u}, d, \bar{d}, c, \bar{c}, s, \bar{s}, b, \bar{b}). \quad (3.18)$$

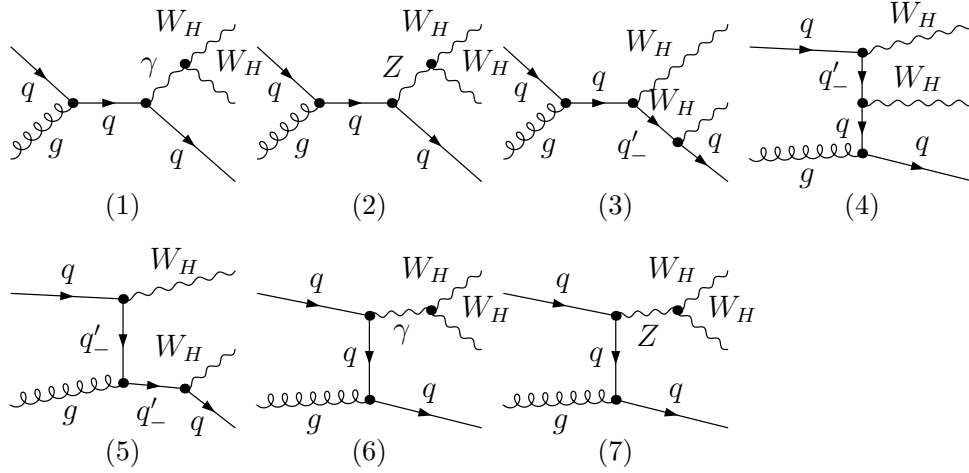


Figure 4: The tree-level Feynman diagrams for real light-quark emission partonic process  $qq \rightarrow W_H^+W_H^- + q$ , ( $q = u, d, c, s, b$ ).

These PDF counterterms can be expressed as

$$\begin{aligned}
\delta G_{q(g)/P}^{(gluon)}(x, \mu_f) &= \frac{1}{\epsilon} \left[ \frac{\alpha_s}{2\pi} \frac{\Gamma(1-\epsilon)}{\Gamma(1-2\epsilon)} \left( \frac{4\pi\mu_r^2}{\mu_f^2} \right)^\epsilon \right] \int_x^1 \frac{dz}{z} P_{qq(gg)}(z) G_{q(g)/P}(x/z, \mu_f), \\
\delta G_{q/P}^{(quark)}(x, \mu_f) &= \frac{1}{\epsilon} \left[ \frac{\alpha_s}{2\pi} \frac{\Gamma(1-\epsilon)}{\Gamma(1-2\epsilon)} \left( \frac{4\pi\mu_r^2}{\mu_f^2} \right)^\epsilon \right] \int_x^1 \frac{dz}{z} P_{qg}(z) G_{g/P}(x/z, \mu_f), \\
\delta G_{g/P}^{(quark)}(x, \mu_f) &= \frac{1}{\epsilon} \left[ \frac{\alpha_s}{2\pi} \frac{\Gamma(1-\epsilon)}{\Gamma(1-2\epsilon)} \left( \frac{4\pi\mu_r^2}{\mu_f^2} \right)^\epsilon \right] \sum_{q=u,\bar{u},d,\bar{d}}^{c,\bar{c},s,\bar{s},b,\bar{b}} \int_x^1 \frac{dz}{z} P_{gq}(z) G_{q/P}(x/z, \mu_f), \quad (3.19)
\end{aligned}$$

where  $P_{ij}(z)$  ( $ij = qq, qg, gq, gg$ ) denote the splitting functions. One can find their explicit expressions in Ref.[32].

### III..2.4 Correction from $gg \rightarrow W_H^+W_H^-$ partonic process

The gluon-gluon fusion partonic process  $gg \rightarrow W_H^+W_H^-$  contributes also to the parent process  $pp \rightarrow W_H^+W_H^- + X$ . We can see that the QCD NLO correction to the partonic process  $q\bar{q} \rightarrow W_H^+W_H^-$  is at the order of  $\alpha_{ew}^2\alpha_s$ , while the lowest order partonic process  $gg \rightarrow W_H^+W_H^-$  is at the order of  $\alpha_{ew}^2\alpha_s^2$ . The later LO contribution is  $\alpha_s$  order higher than the QCD NLO contribution from previous subprocess. But both contribution parts might be comparable with each other due to the large gluon luminosity at the TeV-scale collider LHC. The representative Feynman diagrams for gluon-gluon fusion partonic process are depicted in Fig.5. The total one-loop amplitude  $\mathcal{M}_{gg}^{1-loop}$  for this partonic process is UV

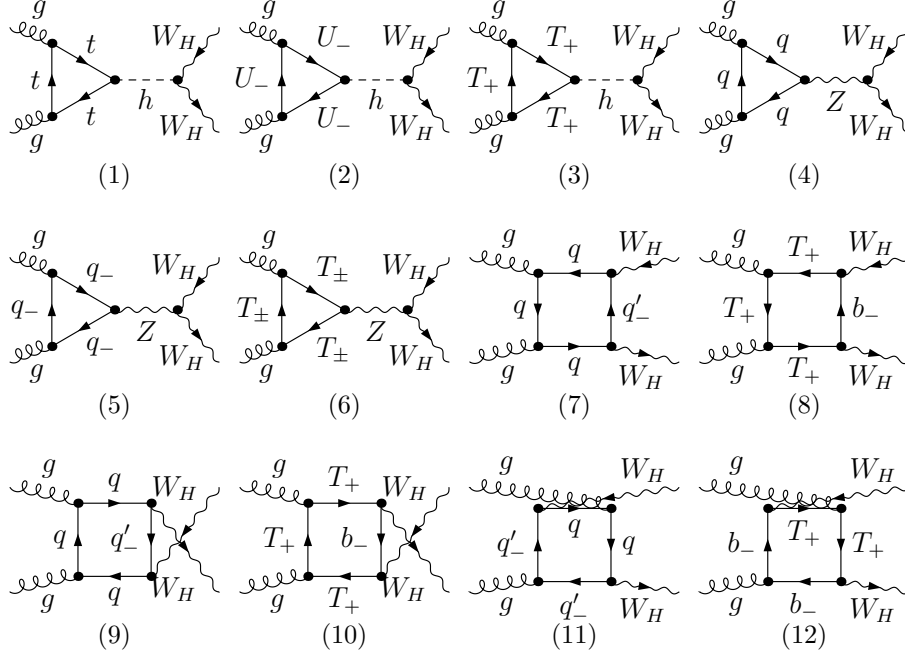


Figure 5: The representative lowest order Feynman diagrams for the partonic process  $gg \rightarrow W_H^+ W_H^-$ , where  $U_- = u_-, c_-, t_-$ ,  $q, q' = u, d, c, s, b, t$  and  $q_-, q'_- = u_-, d_-, c_-, s_-, b_-, t_-$ .

and IR finite, and the cross section at the lowest order,  $\hat{\sigma}_{gg}^0$ , can be expressed as

$$\hat{\sigma}_{gg}^0 = \frac{1}{4} \frac{1}{64} \frac{(2\pi)^4}{4|\vec{p}|\sqrt{\hat{s}}} \int \sum_{spin} \sum_{color} |\mathcal{M}_{gg}^{1-loop}|^2 d\Omega_2. \quad (3.20)$$

The total cross section for the parent process  $pp \rightarrow gg \rightarrow W_H^+ W_H^- + X$  at the lowest order can be obtained by integrating the cross section for partonic process  $\hat{\sigma}_{gg}^0$  with the gluon PDF in proton  $G_{g/P}(x, \mu)$ ,

$$\sigma(pp \rightarrow W_H^+ W_H^- + X) = \frac{1}{2} \int_0^1 dx_1 \int_0^1 dx_2 [G_{g/P_1}(x_1, \mu_f) G_{g/P_2}(x_2, \mu_f) + (1 \leftrightarrow 2)] \hat{\sigma}_{gg}^0(\hat{s} = x_1 x_2 s), \quad (3.21)$$

where we adopt the notations same as in Eq.(3.6).

### III..2.5 Total QCD NLO correction

After the renormalization and summing up all the QCD NLO one-loop corrections, the gluon/light-(anti)quark emission corrections and the PDF counterterm contributions, all the UV and IR (both soft and collinear) singularities are eliminated. Consequently, the QCD NLO corrected integrated cross

section for the  $pp \rightarrow W_H^+ W_H^- + X$  process is finite and can be expressed as

$$\begin{aligned}\sigma_{NLO} &= \sigma_{LO} + \Delta\sigma_{NLO} = \sigma_{LO} + \Delta\sigma^{(2)} + \Delta\sigma^{(3)} \\ &= \sigma_{LO} + \Delta\sigma_{NLO}(pp \rightarrow q\bar{q} \rightarrow W_H^+ W_H^- + X) + \sigma(pp \rightarrow gg \rightarrow W_H^+ W_H^- + X).\end{aligned}\quad (3.22)$$

where  $\Delta\sigma_{NLO}$  consists of two parts,  $\Delta\sigma_{NLO}(pp \rightarrow q\bar{q} \rightarrow W_H^+ W_H^- + X)$  and  $\sigma(pp \rightarrow gg \rightarrow W_H^+ W_H^- + X)$ . The two-body term  $\Delta\sigma^{(2)}$  includes the one-loop corrections to the  $pp \rightarrow q\bar{q} \rightarrow W_H^+ W_H^- + X$  process, the lowest order contribution from the  $pp \rightarrow gg \rightarrow W_H^+ W_H^- + X$  process and the cross sections for the real gluon/light-(anti)quark emission processes over the soft and hard collinear phase-space regions, while the three-body term  $\Delta\sigma^{(3)}$  contains the cross sections for the real gluon/light-(anti)quark emission processes over the hard noncollinear regions.

## IV. Numerical results and discussions

### IV..1 Input parameters

As discussed in Ref.[36], the two mixing matrices satisfy  $V_{Hu}^\dagger V_{Hd} = V_{CKM}$ . Therefore, they cannot simultaneously be set to the identity. In the following calculations we take  $V_{Hu}$  to be a unit matrix, then we have  $V_{Hd} = V_{CKM}$ . We take  $\alpha_{ew}(m_Z^2)^{-1} = 127.916$ ,  $m_W = 80.399 \text{ GeV}$ ,  $m_Z = 91.1876 \text{ GeV}$ ,  $\sin^2 \theta_W = 1 - \left(\frac{m_W}{m_Z}\right)^2 = 0.2226$  and  $m_t = 171.2 \text{ GeV}$  [37]. The masses of all the SM leptons and quarks except top quark are neglected. The center-of-mass energies  $\sqrt{s}$  of proton-proton collision are taken to be  $14 \text{ TeV}$  and  $8 \text{ TeV}$  for the future and early LHC, separately. We set the factorization and renormalization scale to be equal ( $\mu_r = \mu_f$ ) and define  $\mu_0 = m_{W_H}$ . We employ CTEQ6L1 and CTEQ6M in the the LO and NLO calculations respectively [38], and fix the LHT parameters  $\kappa = 1$  and  $s_\alpha = c_\alpha = \frac{\sqrt{2}}{2}$ . Then the masses of heavy gauge bosons and  $T$ -odd quarks are only the functions of the LHT parameter  $f$  as shown in Eqs.(2.4) and (2.7). The Cabibbo-Kobayashi-Maskawa (CKM) matrix elements are taken as

$$V_{CKM} = \begin{pmatrix} V_{ud} & V_{us} & V_{ub} \\ V_{cd} & V_{cs} & V_{cb} \\ V_{td} & V_{ts} & V_{tb} \end{pmatrix} = \begin{pmatrix} 0.97418 & 0.22577 & 0 \\ -0.22577 & 0.97418 & 0 \\ 0 & 0 & 1 \end{pmatrix}. \quad (4.1)$$

### IV..2 Masses and Decay widths

From Eq.(2.7) we can see that all the  $T$ -odd quarks  $q_-$  ( $q_- = u_-, d_-, s_-, c_-, b_-, t_-$ ) have nearly equal masses when the scale  $f$  is large enough. By using Eqs.(2.4), (2.7), (2.12) and (2.15), and taking the

$f$ (GeV)	$m_{W_H} \approx m_{Z_H}$ (GeV)	$m_{u_-} = m_{c_-} = m_{t_-}$ (GeV)	$m_{d_-} = m_{s_-} = m_{b_-}$ (GeV)	$m_{T_+}$ (GeV)	$m_{T_-}$ (GeV)
500	322.1	685.7	707.1	695.9	507.0
700	457.8	974.7	989.9	974.3	699.6
800	525.1	1118.0	1131.4	1113.5	796.7
900	592.3	1260.9	1272.8	1252.7	894.1
1100	726.1	1545.9	1555.6	1531.1	1089.4
1300	859.7	1830.3	1838.5	1809.4	1285.2
1500	993.1	2114.2	2121.3	2087.8	1481.3

Table 1: The masses of  $W_H$ ,  $q_-$  ( $q_- = u_-, d_-, c_-, s_-, b_-, t_-$ ) and  $T_{\pm}$  for some typical values of the LHT parameter  $f$  with  $\kappa = 1$  and  $s_{\alpha} = c_{\alpha} = \frac{\sqrt{2}}{2}$ .

LHT parameters  $\kappa = 1$  and  $s_{\alpha} = c_{\alpha} = \frac{\sqrt{2}}{2}$ , we obtain the masses of heavy gauge bosons,  $T$ -odd quarks and the quarks in top sector for some typical values of the LHT global symmetry breaking scale  $f$ , and list them in Table 1.

With above related parameters and Eqs.(6.1) and (6.2) in Appendix B, we obtain numerically the LO decay widths  $\Gamma_{q_-}$  as functions of  $f$  in Fig.6, where we give only the curves for  $U_- = u_-, c_-$ ,  $D_- = d_-, s_-$  and  $t_-$ -quarks. The decay width of the  $T$ -odd  $b_-$ -quark is not presented in the figure, since it is not relevant in our calculations.

### IV..3 Checks

The correctness of our calculations are verified in the following aspects:

1. We adopt the same input parameters and PDFs as used in Ref.[24], and compare our LO results with those as shown in Fig.9 of Ref.[24]. We find that our LO cross sections are in good agreement with those read out from the figure.
2. The cancelations of UV and IR divergences are verified numerically after combining all the contributions at the QCD NLO.
3. The one-loop virtual corrections are computed independently by using two different programs. One is based on our in-house codes for numerical evaluation of the one-loop integrals, and the other is LoopTools 2.2 package. We find that the numerical results coincide with each other within the calculation errors.

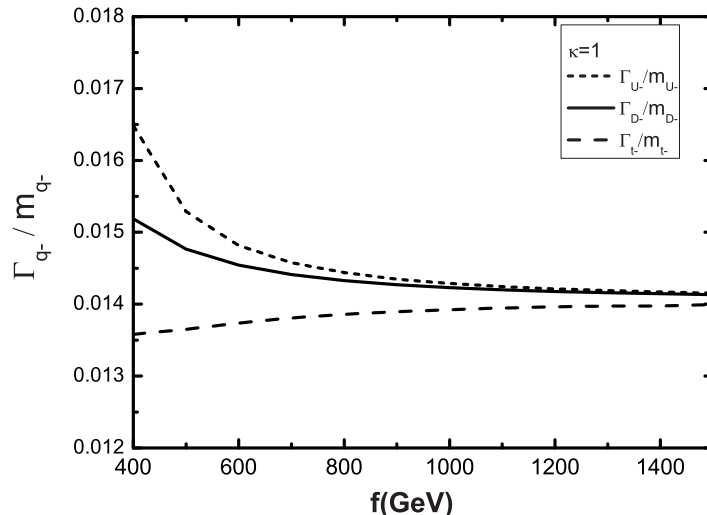


Figure 6: The LO total decay widths of the  $T$ -odd quarks as functions of the global symmetry breaking scale  $f$ , where  $q_- = U_-, D_-, t_-$  and  $(U_-, D_-) = (u_-, d_-), (c_-, s_-)$ .

4. The  $\delta_s/\delta_c$  independence of the total QCD NLO correction has been numerically verified. As mentioned above, in the TCPSS method two arbitrary cutoffs are introduced to separate the phase-space in order to isolate the IR divergences. From Eq.(3.22), the total QCD NLO correction ( $\Delta\sigma_{NLO}$ ) can be divided into the two-body and three-body corrections ( $\Delta\sigma^{(2)}$  and  $\Delta\sigma^{(3)}$ ) by the two cutoffs. We depict  $\Delta\sigma^{(2)}$ ,  $\Delta\sigma^{(3)}$  and  $\Delta\sigma_{NLO}$  for the process  $pp \rightarrow u\bar{u} \rightarrow W_H^+ W_H^- + X$  as functions of the soft cutoff  $\delta_s$  in Fig.7(a) with  $f = 800 \text{ GeV}$ ,  $\kappa = 1$ ,  $s_\alpha = c_\alpha = \frac{\sqrt{2}}{2}$ ,  $\delta_c = \delta_s/100$  and  $\mu = \mu_0 = m_{W_H} = 525.15 \text{ GeV}$ . The amplified curve for the total correction  $\Delta\sigma_{NLO}$  in Fig.7(a) is demonstrated in Fig.7(b) together with calculation errors. We adopt also the dipole subtraction (DPS) method [39] to deal with the IR singularities for further verification. The  $\Delta\sigma_{NLO}$  result by adopting this method with  $\pm 1\sigma$  statistic error is plotted as the shadowing region in Fig.7(b). We can see that the results from both the TCPSS method and the DPS method are in good agreement. From these two figures we find that the total QCD NLO correction  $\Delta\sigma_{NLO}$  is independent of the two cutoffs within the statistical errors. This independence is an indirect check for the correctness of our work. In further numerical calculations, we fix  $\delta_s = 1 \times 10^{-4}$  and  $\delta_c = 1 \times 10^{-6}$ .

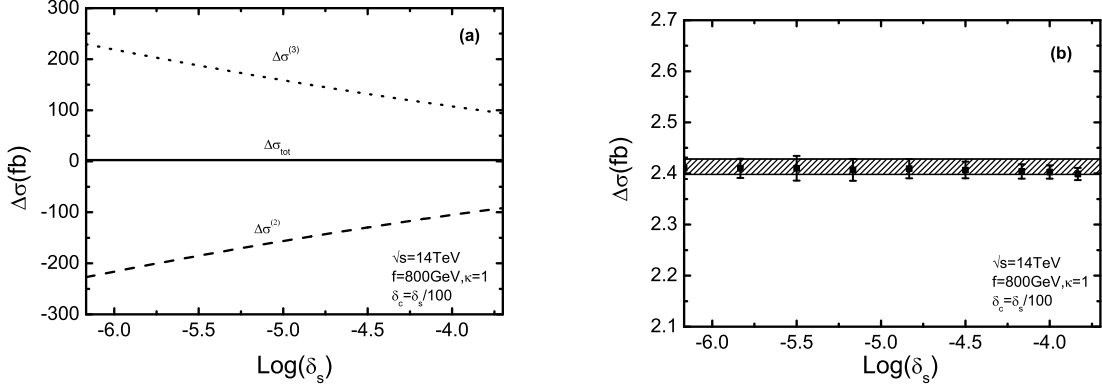


Figure 7: (a) The dependence of the QCD NLO corrections to the  $pp \rightarrow u\bar{u} \rightarrow W_H^+ W_H^- + X$  process on the cutoffs  $\delta_s$  and  $\delta_c$  at the  $\sqrt{s} = 14 \text{ TeV}$  LHC, where we take  $f = 800 \text{ GeV}$ ,  $\kappa = 1$ ,  $s_\alpha = c_\alpha = \frac{\sqrt{2}}{2}$ ,  $\delta_c = \delta_s/100$  and  $\mu = \mu_0 = m_{W_H} = 525.15 \text{ GeV}$ . (b) The amplified curve for  $\Delta\sigma_{tot}$  in Fig.7(a). The shadowing region shows the result by adopting DPS method with  $\pm 1\sigma$  statistic error.

#### IV..4 Dependence on factorization/renormalization scale

In Figs.8(a,b) we present the dependence of the LO, QCD NLO corrected integrated cross sections and the corresponding  $K$ -factor ( $K \equiv \sigma_{NLO}/\sigma_{LO}$ ) on the factorization/renormalization scale  $\mu$  for the process  $pp \rightarrow W_H^+ W_H^- + X$  at the  $\sqrt{s} = 14 \text{ TeV}$  and the  $\sqrt{s} = 8 \text{ TeV}$  LHC separately, where we take the LHT parameters  $f = 800 \text{ GeV}$ ,  $\kappa = 1$  and  $s_\alpha = c_\alpha = \frac{\sqrt{2}}{2}$ . From the curves in Figs.8(a,b), we find that QCD NLO corrections to the  $pp \rightarrow W_H^+ W_H^- + X$  process significantly reduce the scale uncertainty. We can read out from the figures that the LO and QCD NLO corrected cross sections at  $\mu_0 = m_{W_H}$  are  $\sigma_{LO}(\sqrt{s} = 14 \text{ TeV}) = 32.63_{-6.38}^{+9.56} \text{ fb}$ ,  $\sigma_{NLO}(\sqrt{s} = 14 \text{ TeV}) = 37.43_{-2.83}^{+2.19} \text{ fb}$  and  $\sigma_{LO}(\sqrt{s} = 8 \text{ TeV}) = 5.54_{-1.51}^{+2.71} \text{ fb}$ ,  $\sigma_{NLO}(\sqrt{s} = 8 \text{ TeV}) = 6.14_{-0.70}^{+0.26} \text{ fb}$ , where the uncertainties describe the missing higher-order corrections estimated via scale variations in the range of  $0.1\mu_0 < \mu < 10\mu_0$ . The  $K$ -factor varies from 0.94 (0.77) to 1.32 (1.35) at the  $\sqrt{s} = 14 \text{ TeV}$  (8 TeV) LHC, when  $\mu/\mu_0$  goes from 0.1 to 10. With the definition of scale uncertainty as  $\eta = \frac{|\sigma(0.1\mu_0) - \sigma(10\mu_0)|}{\sigma(\mu_0)}$ , we obtain that the scale uncertainties are reduced from 48.88% (LO) to 13.40% (NLO) at the  $\sqrt{s} = 14 \text{ TeV}$  and from 76.23% (LO) to 14.54% (NLO) at the  $\sqrt{s} = 8 \text{ TeV}$  LHC, respectively. In Table 2 we list some numerical results of the cross sections and  $K$ -factors for some typical values of  $\mu/\mu_0$ , which are read out from Figs.8(a,b). In order to investigate the contribution from the  $pp \rightarrow gg \rightarrow W_H^+ W_H^- + X$  process, which

$\sqrt{s}$ (TeV)	$\mu/\mu_0$	$\sigma_{LO}$ (fb)	$\sigma_{NLO}$ (fb)	$\sigma(gg)$ (fb)	$K$
14	0.1	42.190(1)	39.62(2)	0.993(1)	0.939
	0.5	35.091(1)	38.17(2)	0.3946(6)	1.09
	1	32.626(1)	37.43(2)	0.2810(5)	1.15
	2	30.444(1)	37.53(2)	0.2056(4)	1.20
	10	26.242(1)	34.60(2)	0.1081(2)	1.32
8	0.1	8.2548(4)	6.333(3)	0.0805(1)	0.767
	0.5	6.1850(3)	6.300(3)	0.02842(3)	1.019
	1	5.5417(2)	6.143(3)	0.01943(3)	1.11
	2	5.0006(2)	5.947(3)	0.01371(2)	1.21
	10	4.0304(2)	5.440(2)	0.00671(1)	1.40

Table 2: The numerical results of  $\sigma_{LO}$ ,  $\sigma_{NLO}$  and the corresponding  $K$ -factors at the 14 TeV and the 8 TeV LHC by taking  $f = 800$  GeV,  $\kappa = 1$ ,  $s_\alpha = c_\alpha = \frac{\sqrt{2}}{2}$  and some typical values of factorization/renormalization scale  $\mu$ .  $\sigma(gg)$  is the cross section for the  $pp \rightarrow gg \rightarrow W_H^+ W_H^- + X$  process, which is considered as a component of the QCD NLO correction to the parent process  $pp \rightarrow W_H^+ W_H^- + X$ .

is considered as a component of the QCD NLO corrections to the parent process  $pp \rightarrow W_H^+ W_H^- + X$ , we also present the cross sections for the  $pp \rightarrow gg \rightarrow W_H^+ W_H^- + X$  process ( $\sigma(gg)$ ) in this table. We can obtain from the data that the QCD NLO correction part from the  $pp \rightarrow gg \rightarrow W_H^+ W_H^- + X$  process at  $\mu = \mu_0$  is about 5.85% (3.23%) of the total QCD NLO correction ( $\Delta\sigma_{NLO}$ ) at the 14 TeV (8 TeV) LHC. We can see also that the NLO theoretical uncertainty due the choice of  $\mu$  mainly comes from the genuine QCD NLO corrected cross section for the  $pp \rightarrow q\bar{q} \rightarrow W_H^+ W_H^- + X$  process, while the contribution from the  $pp \rightarrow gg \rightarrow W_H^+ W_H^- + X$  process is relatively small. In further numerical calculations we fix the renormalization and factorization scales being equal to their central value, i.e.,  $\mu = \mu_r = \mu_f = \mu_0 = m_{W_H}$ .

#### IV..5 Dependence on global symmetry breaking scale $f$

The LO and QCD NLO corrected integrated cross sections together with the corresponding  $K$ -factor as functions of the scale  $f$  at the  $\sqrt{s} = 14$  TeV and the  $\sqrt{s} = 8$  TeV LHC are depicted in Figs.9(a) and (b), respectively. We can see from Fig.9 that the LO and NLO total cross sections for the  $pp \rightarrow W_H^+ W_H^- + X$  process decrease drastically when  $f$  goes up. This is because the mass of final  $W_H$  becomes heavier as the increment of  $f$ , therefore the phase-space becomes smaller. We can read

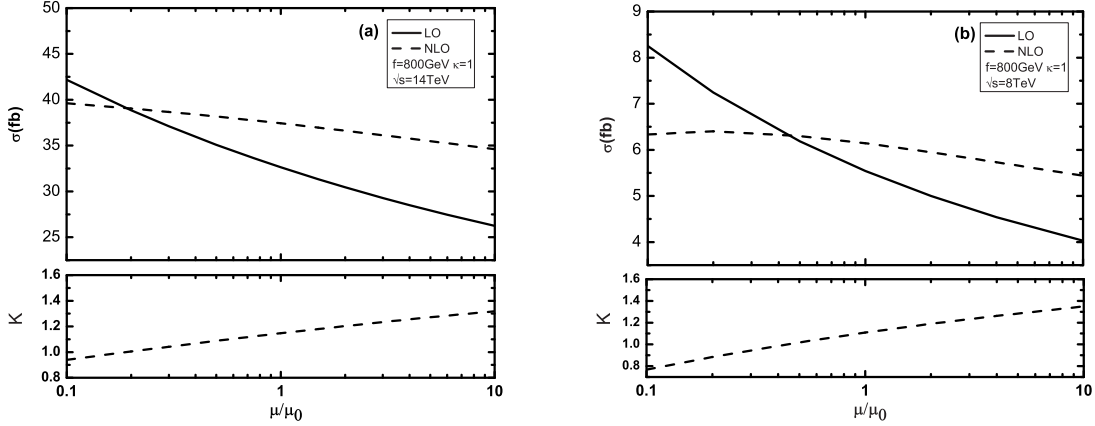


Figure 8: The dependence of the LO, QCD NLO corrected integrated cross sections and the corresponding  $K$ -factors for the  $pp \rightarrow W_H^+ W_H^- + X$  process on the factorization/renormalization scale  $\mu$  at the LHC with  $f = 800 \text{ GeV}$ ,  $\kappa = 1$  and  $s_\alpha = c_\alpha = \frac{\sqrt{2}}{2}$ . (a)  $\sqrt{s} = 14 \text{ TeV}$ . (b)  $\sqrt{s} = 8 \text{ TeV}$ .

out from the figures that the corresponding  $K$ -factor varies from 1.22 to 1.10 at the  $\sqrt{s} = 14 \text{ TeV}$  LHC and from 1.17 to 1.10 at the  $\sqrt{s} = 8 \text{ TeV}$  LHC in the plotted  $f$  range. In Table 3, we list some numerical results of the LO, NLO cross sections and the corresponding  $K$ -factors for some typical values of  $f$  which are shown in Figs.9(a,b).

#### IV..6 Differential cross sections

In this subsection, we investigate the kinematic distributions of final products after the subsequential decays of heavy charged gauge bosons ( $W_H^+ \rightarrow W^+ A_H \rightarrow e^+ \nu_e A_H$  and  $W_H^- \rightarrow W^- A_H \rightarrow \mu^- \bar{\nu}_\mu A_H$ ). We take the branching ratio of the  $W_H$  boson decay as  $Br(W_H \rightarrow W A_H) = 100\%$  for  $\kappa = 1$  and  $f = 800 \text{ GeV}$  [24], and the branching ratios of the  $W$  boson decay as  $Br(W^+ \rightarrow e^+ \nu_e) = 10.75\%$  and  $Br(W^- \rightarrow \mu^- \bar{\nu}_\mu) = 10.57\%$  [37]. The  $W_H$ -pair production channel including their subsequential decays can be written as

$$pp \rightarrow W_H^+ W_H^- \rightarrow W^+ W^- A_H A_H \rightarrow e^+ \nu_e \mu^- \bar{\nu}_\mu A_H A_H. \quad (4.2)$$

Then a signal event of  $W_H$ -pair production is detected at the LHC as two charged leptons ( $e^+$  and  $\mu^-$ ) plus missing energy ( $A_H A_H \nu_e \bar{\nu}_\mu$ ). In Figs.10(a) and (b) we present the LO, QCD NLO corrected distributions of the transverse momentum of  $W^+$ , and the corresponding  $K$ -factors at the  $\sqrt{s} = 14 \text{ TeV}$

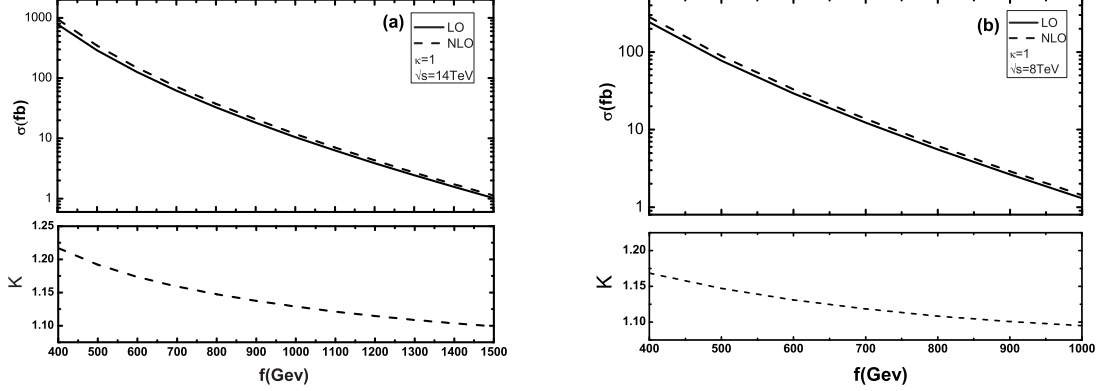


Figure 9: The LO, QCD NLO corrected integrated cross sections and the corresponding  $K$ -factors for the  $pp \rightarrow W_H^+ W_H^- + X$  process as the functions of the global symmetry breaking scale  $f$  at the LHC with  $\kappa = 1$  and  $s_\alpha = c_\alpha = \frac{\sqrt{2}}{2}$ . (a)  $\sqrt{s} = 14 \text{ TeV}$ . (b)  $\sqrt{s} = 8 \text{ TeV}$ .

$\sqrt{s}$ (TeV)	$f$ (GeV)	$\sigma_{LO}$ (fb)	$\sigma_{NLO}$ (fb)	$K$
14	500	289.93(1)	345.6(2)	1.19
	700	62.053(3)	71.93(4)	1.16
	800	32.626(1)	37.43(2)	1.15
	900	18.1252(8)	20.61(1)	1.14
	1100	6.2964(3)	7.059(3)	1.12
	1300	2.44312(9)	2.709(1)	1.11
	1500	1.02314(4)	1.1246(5)	1.10
8	500	77.693(3)	89.12(5)	1.15
	700	12.2863(5)	13.741(7)	1.12
	800	5.5417(2)	6.143(3)	1.11
	900	2.6357(1)	2.901(1)	1.10

Table 3: The numerical results of  $\sigma_{LO}$ ,  $\sigma_{NLO}$  and the corresponding  $K$ -factors at the  $\sqrt{s} = 14 \text{ TeV}$  and the  $\sqrt{s} = 8 \text{ TeV}$  LHC by taking  $\kappa = 1$ ,  $s_\alpha = c_\alpha = \frac{\sqrt{2}}{2}$ ,  $\mu = \mu_0$  and some typical values of  $f$ .

and the  $\sqrt{s} = 8 \text{ TeV}$  LHC, separately. From Figs.10(a,b) we can see that the QCD corrections always enhance the LO differential cross section  $d\sigma_{LO}/dp_T^{W^+}$ , and both the LO and QCD NLO corrected distributions of final  $W^+$  boson at the future and the early LHC have their peaks around the position of  $p_T^{W^+} \sim 180 \text{ GeV}$ , and the  $K$ -factors are all less than 1.20.

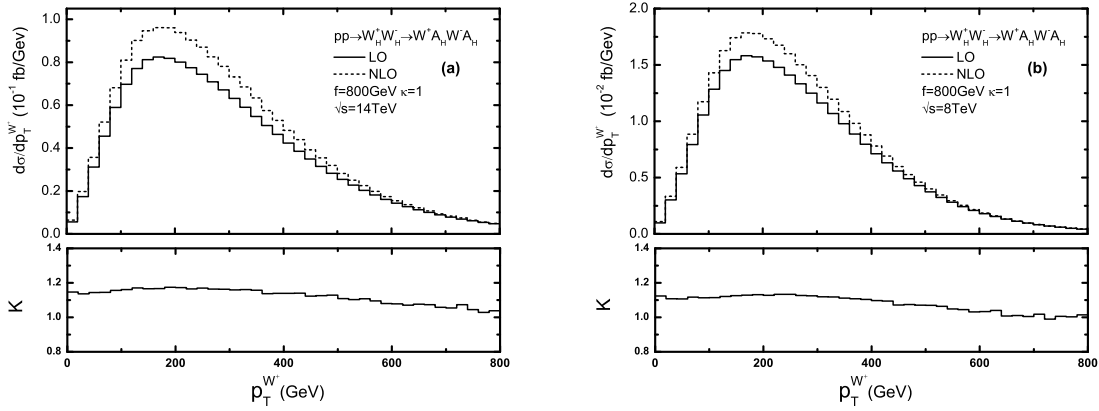


Figure 10: The LO, QCD NLO corrected  $p_T^{W^+}$  distributions and the corresponding  $K$ -factors of final  $W^+$  boson for the  $pp \rightarrow W_H^+ W_H^- + X$  process at the LHC by taking  $f = 800 \text{ GeV}$ ,  $\kappa = 1$  and  $s_\alpha = c_\alpha = \frac{\sqrt{2}}{2}$ . (a)  $\sqrt{s} = 14 \text{ TeV}$ . (b)  $\sqrt{s} = 8 \text{ TeV}$ .

Since we neglect the masses of both positron and  $\mu^-$  in numerical calculations, the distribution of the positron transverse momentum should be the same as  $\mu^-$ . The LO, QCD NLO corrected distributions of the final lepton ( $e^+/\mu^-$ ) transverse momentum and missing transverse momentum of  $A_H A_H \nu_e \bar{\nu}_\mu$ , and the corresponding  $K$ -factors are depicted in Figs.11(a,b,c,d) at the  $\sqrt{s} = 14 \text{ TeV}$  and the  $\sqrt{s} = 8 \text{ TeV}$  LHC, separately. From Figs.11(a,b) we can see that the peaks on the  $d\sigma_{LO}/dp_T^{e^+/\mu^-}$  and  $d\sigma_{NLO}/dp_T^{e^+/\mu^-}$  curves are all located at the vicinity of  $p_T \sim 30 \text{ GeV}$ . Figs.11(c,d) show that the LO and NLO missing transverse momentum distributions reach their maxima at  $p_T^{miss} \sim 110 \text{ GeV}$ , and the  $K$ -factors are between 0.86 and 1.65 at the  $\sqrt{s} = 14 \text{ TeV}$  LHC, and between 0.91 and 1.24 at the  $\sqrt{s} = 8 \text{ TeV}$  LHC in the plotted range, respectively. All the figures in Figs.10(a,b) and Figs.11(a,b) show that the LO differential cross sections,  $\frac{d\sigma_{LO}}{dp_T^{W^+}}$ ,  $\frac{d\sigma_{LO}}{dp_T^{e^+/\mu^-}}$ , at the early and the future LHC, are enhanced by the QCD NLO calculations considerably in the plotted  $p_T$  regions, while the distributions of  $p_T^{miss}$  in Figs.11(c,d) for the  $14 \text{ TeV}$  and the  $8 \text{ TeV}$  LHC, show that the QCD NLO corrections decrease the LO differential cross sections in the low  $p_T^{miss}$  region.

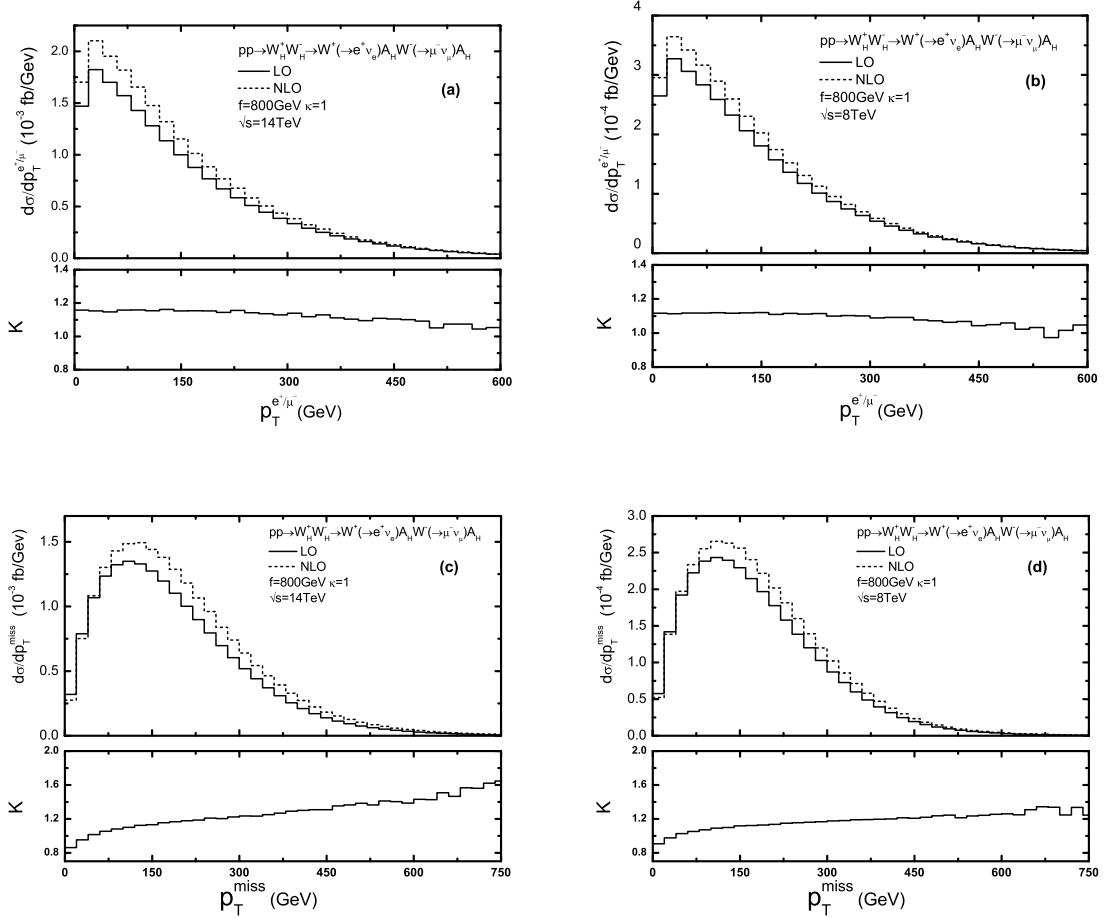


Figure 11: The LO, QCD NLO corrected transverse momentum distributions of final particles and the corresponding  $K$ -factors of the  $pp \rightarrow W_H^+ W_H^- \rightarrow e^+ \mu^- A_H A_H \nu_e \bar{\nu}_\mu$  process at the LHC by taking  $f = 800$  GeV,  $\kappa = 1$  and  $s_\alpha = c_\alpha = \frac{\sqrt{2}}{2}$ . (a)  $e^+/\mu^-$  transverse momentum distribution at the  $\sqrt{s} = 14$  TeV LHC. (b)  $e^+/\mu^-$  transverse momentum distribution at the  $\sqrt{s} = 8$  TeV LHC. (c) missing transverse momentum distribution at the  $\sqrt{s} = 14$  TeV LHC. (d) missing transverse momentum distribution at the  $\sqrt{s} = 8$  TeV LHC.

In Figs.12(a,b), we present the the LO, QCD NLO corrected distributions of the azimuthal angle between  $e^+$  and  $\mu^-$  and the corresponding  $K$ -factors for the  $pp \rightarrow W_H^+ W_H^- \rightarrow e^+ \mu^- A_H A_H \nu_e \bar{\nu}_\mu$  process at the LHC, where we take  $f = 800 \text{ GeV}$ ,  $\kappa = 1$  and  $s_\alpha = c_\alpha = \frac{\sqrt{2}}{2}$  at the future  $\sqrt{s} = 14 \text{ TeV}$  LHC and the present  $\sqrt{s} = 8 \text{ TeV}$  LHC, separately. The azimuthal angle between  $e^+$  and  $\mu^-$  is obtained by using the following equation:

$$\varphi^{(e^+ \mu^-)} = \arccos \left( \frac{\vec{p}_T^{e^+} \cdot \vec{p}_T^{\mu^-}}{|\vec{p}_T^{e^+}| |\vec{p}_T^{\mu^-}|} \right), \quad (4.3)$$

where  $\vec{p}_T^{e^+}$  and  $\vec{p}_T^{\mu^-}$  are the three-momenta of  $e^+$  and  $\mu^-$ . From the figures we can see that the majority of the  $W_H$ -pair production events tends to have their final leptons  $e^+$  and  $\mu^-$  outgoing back to back on the transverse plane. That feature could explain the fact that the QCD NLO correction decreases the LO differential cross section of  $d\sigma_{LO}/dp_T^{miss}$  in the low  $p_T^{miss}$  region as shown in Figs.11(c,d). As we know from Fig.7(a) that the correction part of  $\Delta\sigma^{(2)}$  is usually negative, while the hard noncollinear real emission correction part  $\Delta\sigma^{(3)}$  is positive. The contribution of three-body term from the real emission process  $pp \rightarrow W_H^+ W_H^- + \text{jet} \rightarrow e^+ \mu^- + E_{\text{miss}} + \text{jet}$  would kinematically suppress  $d\sigma/dp_T^{miss}$  in low  $p_T^{miss}$  region comparing with the  $p_T^{miss}$  distribution of the  $pp \rightarrow W_H^+ W_H^- \rightarrow e^+ \mu^- + E_{\text{miss}}$  events due to the majority of the final leptons  $e^+$  and  $\mu^-$  outgoing back to back on the transverse plane.

The LO and QCD NLO corrected distributions of the invariant mass of final leptons,  $e^+$  and  $\mu^-$ , are demonstrate in Figs.13(a,b), where Figs.13(a) and (b) are for the distributions of the invariant mass  $M_{(e^+ \mu^-)}$  and the corresponding  $K$ -factors at the  $\sqrt{s} = 14 \text{ TeV}$  and the  $\sqrt{s} = 8 \text{ TeV}$  LHC, respectively. We see from Figs.13(a,b) that both LO and NLO curves for the differential cross sections reach their maxima at the vicinity of  $M_{(e^+ \mu^-)} \sim 100 \text{ GeV}$ .

As we know if the kinematic distribution of signal events is distinctively different from that of background events, we can use that feature to significantly suppress the background. For the signal events of the  $pp \rightarrow W_H^+ W_H^- \rightarrow e^+ \mu^- A_H A_H \nu_e \bar{\nu}_\mu$  process, the dominant background at the LHC comes from the SM process  $pp \rightarrow W^+ W^- \rightarrow e^+ \mu^- \nu_e \bar{\nu}_\mu + X$ , which includes the same final leptons ( $e^+$  and  $\mu^-$ ) and missing transverse momentum  $p_T^{miss}$  due to final  $\nu_e \bar{\nu}_\mu$  products [28]. In order to show the impact of the NLO corrections to the kinematic distributions, and compare the distribution line shapes of signal and background, we make the normalization procedure by dividing the differential cross section by its LO total cross section. We plot the normalized distributions of various kinematic observables of

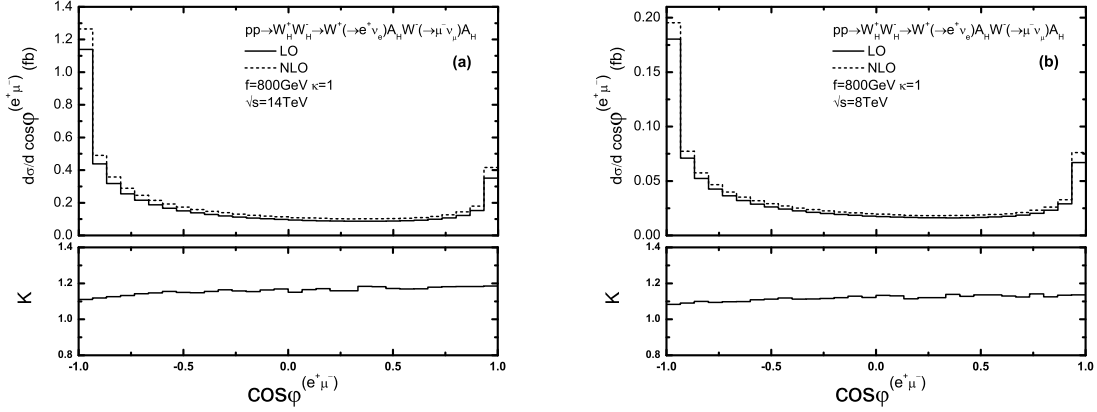


Figure 12: The LO, QCD NLO distributions of  $\cos \varphi^{(e^+ \mu^-)}$ , where  $\varphi^{(e^+ \mu^-)}$  is the azimuthal angle between leptons  $e^+$  and  $\mu^-$ , and the corresponding  $K$ -factors of the  $pp \rightarrow W_H^+ W_H^- \rightarrow e^+ \mu^- A_H A_H \nu_e \bar{\nu}_\mu$  process at the LHC by taking  $f = 800 \text{ GeV}$ ,  $\kappa = 1$  and  $s_\alpha = c_\alpha = \frac{\sqrt{2}}{2}$ . (a)  $\sqrt{s} = 14 \text{ TeV}$ . (b)  $\sqrt{s} = 8 \text{ TeV}$ .

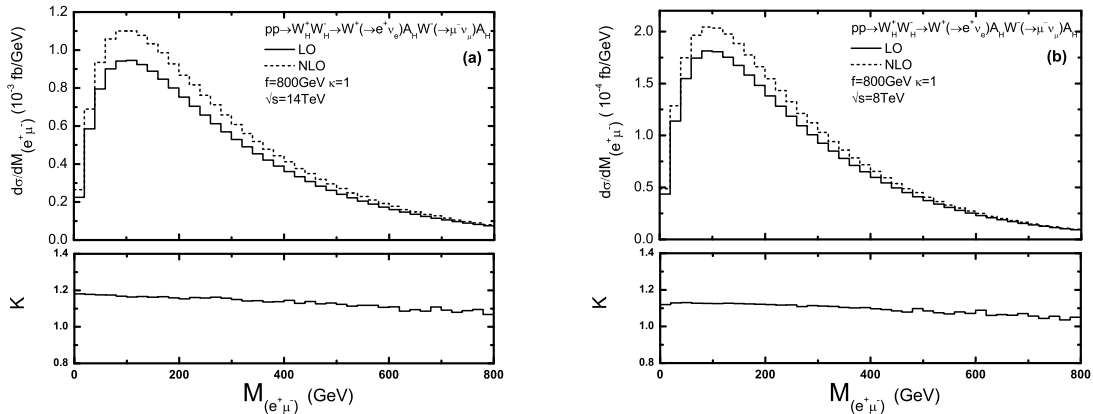


Figure 13: The LO, QCD NLO distributions of invariant mass of final positron and  $\mu^-$ ,  $M_{(e^+ \mu^-)}$ , and the corresponding  $K$ -factors for the  $pp \rightarrow W_H^+ W_H^- \rightarrow e^+ \mu^- A_H A_H \nu_e \bar{\nu}_\mu$  process at the LHC by taking  $f = 800 \text{ GeV}$ ,  $\kappa = 1$  and  $s_\alpha = c_\alpha = \frac{\sqrt{2}}{2}$ . (a)  $\sqrt{s} = 14 \text{ TeV}$ . (b)  $\sqrt{s} = 8 \text{ TeV}$ .

the signal of the  $W_H^+W_H^-$  pair production and its background in Figs.14(a-f) by taking  $f = 800 \text{ GeV}$ ,  $\kappa = 1$  and  $s_\alpha = c_\alpha = \frac{\sqrt{2}}{2}$ . Figs.14(a,c) and Figs.14(b,d) are for the  $p_T$  distributions of final lepton  $e^+/\mu^-$  and undetectable particles at the  $\sqrt{s} = 14 \text{ TeV}$  and the  $\sqrt{s} = 8 \text{ TeV}$  LHC, separately. In Figs.14(e,f) we show the normalized invariant mass  $M_{(e^+\mu^-)}$  distributions at the  $\sqrt{s} = 14 \text{ TeV}$  and the  $\sqrt{s} = 8 \text{ TeV}$  LHC, respectively. We demonstrate the LO and QCD NLO corrected distributions of  $p_T^{e^+/\mu^-}$ ,  $p_T^{miss}$  and  $M_{(e^+\mu^-)}$ , together with the corresponding normalized LO background distributions from  $pp \rightarrow W^+W^- \rightarrow e^+\mu^-\nu_e\bar{\nu}_\mu + X$  process. From those six figures, we can see that the QCD NLO corrections obviously correct the LO differential cross sections of final charged leptons, missing transverse momentum and invariant mass  $M_{(e^+\mu^-)}$  of the signal process, but do not change their LO distribution line shapes very much. We see also that the distributions of the background process  $pp \rightarrow W^+W^- \rightarrow e^+\mu^-\nu_e\bar{\nu}_\mu$  tend to be concentrated in the low  $p_T$  or low  $M_{(e^+\mu^-)}$  range, while the signal distributions can extend to more energetic ranges. Therefore, it is possible to select the signal events of the  $W_H$ -pair production from its background by taking proper  $p_T$  or  $M_{(e^+\mu^-)}$  lower limits on the final charged leptons and the missing transverse momentum. From Figs.14(a-f) we can see if we take proper lower limits on  $p_T^{e^+/\mu^-}$ ,  $p_T^{miss}$  and  $M_{(e^+\mu^-)}$ , the background from  $pp \rightarrow W^+W^- \rightarrow e^+\mu^-\nu_e\bar{\nu}_\mu + X$  process can be significantly suppressed.

## V. Summary

In this work, we present the calculation of the  $W_H$ -pair production at the  $\sqrt{s} = 14 \text{ TeV}$  and the  $\sqrt{s} = 8 \text{ TeV}$  LHC in QCD NLO. The dependence of the total cross section on the renormalization/factorization scale shows that the QCD NLO corrections reduce significantly the uncertainty of the LO theoretical predictions from 48.88% (76.23%) to 13.40% (14.54%) in the range of  $\mu \in [0.1\mu_0, 10\mu_0]$  at the  $\sqrt{s} = 14 \text{ TeV}$  (8 TeV) LHC. Our numerical results demonstrate that the QCD NLO corrections enhance the LO integrated cross sections with a  $K$ -factor in the range of 1.10 – 1.22 (1.09 – 1.17) as the global symmetry breaking scale  $f$  varying from 400 GeV (400 GeV) to 1.5 TeV (1.0 TeV) at the  $\sqrt{s} = 14 \text{ TeV}$  (8 TeV) LHC. We also investigate the kinematic distributions of the transverse momenta of final  $W$  boson, charged leptons and the missing transverse momentum. We find that by putting proper lower limits on  $p_T$ ,  $M_{(e^+\mu^-)}$  of the final leptons and the missing transverse

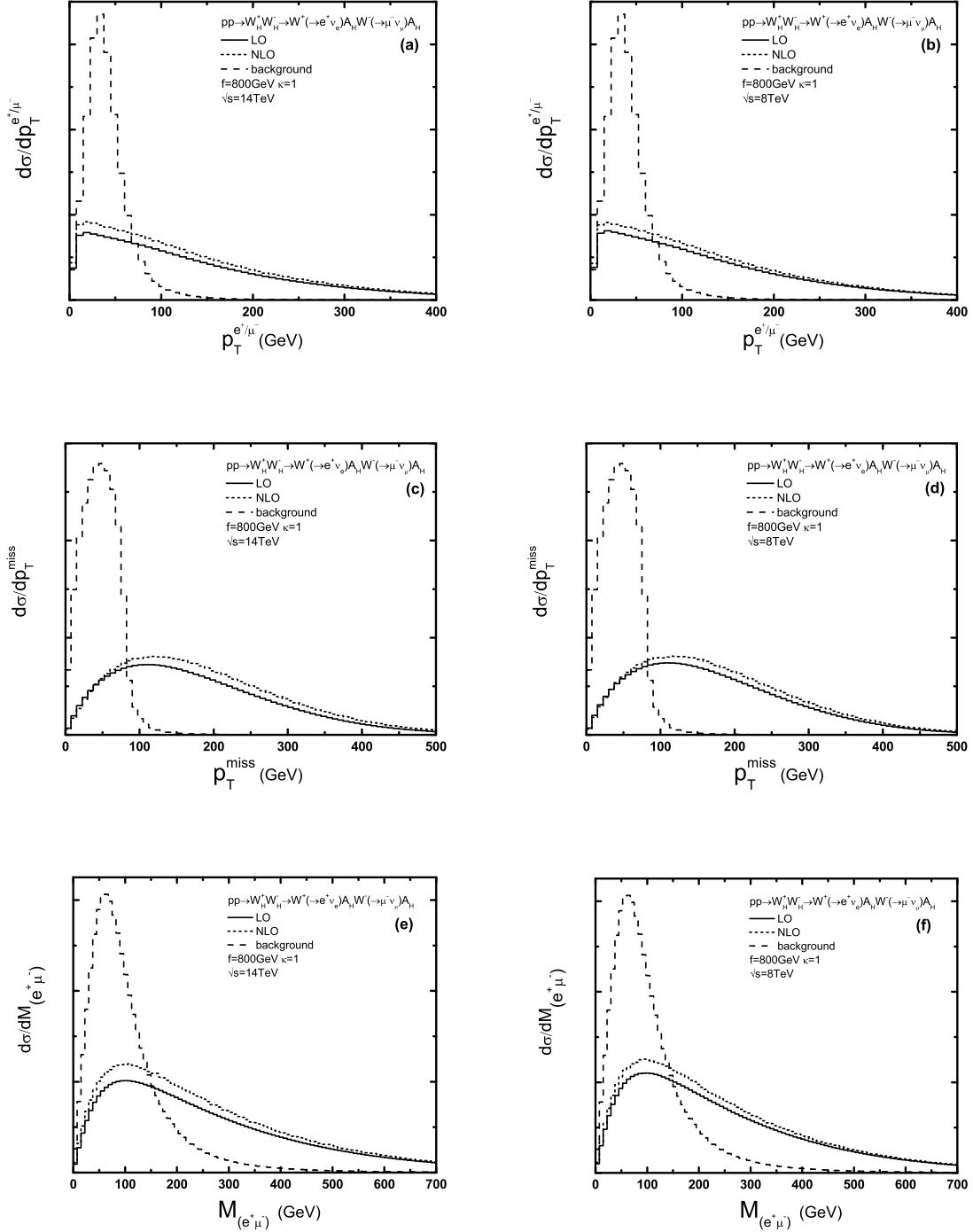


Figure 14: The LO, QCD NLO corrected distributions of transverse momenta of final particles and the distribution of invariant mass  $M_{(e^+\mu^-)}$  of the signal process by taking  $f = 800\text{ GeV}$ ,  $\kappa = 1$  and  $s_\alpha = c_\alpha = \frac{\sqrt{2}}{2}$ . The background is from  $pp \rightarrow W^+W^- \rightarrow e^+\mu^-\nu_e\bar{\nu}_\mu$  process, and all curves in Figs.14 are normalized by their total cross sections. (a)  $p_T$  distribution of final lepton  $e^+/\mu^-$  at the  $\sqrt{s} = 14\text{ TeV}$  LHC. (b)  $p_T$  distribution of final lepton  $e^+/\mu^-$  at the  $\sqrt{s} = 8\text{ TeV}$  LHC. (c) missing transverse momentum distribution at the  $\sqrt{s} = 14\text{ TeV}$  LHC. (d) missing transverse momentum distribution at the  $\sqrt{s} = 8\text{ TeV}$  LHC. (e)  $M_{(e^+\mu^-)}$  distributions at the  $\sqrt{s} = 14\text{ TeV}$  LHC. (f)  $M_{(e^+\mu^-)}$  distributions at the  $\sqrt{s} = 8\text{ TeV}$  LHC. 26

momentum it is possible to select the signal events of the  $W_H$ -pair production from its background with high ratio of signature to background.

**Acknowledgments:** This work was supported in part by the National Natural Science Foundation of China (Contract No.11075150, No.11005101), and the Specialized Research Fund for the Doctoral Program of Higher Education (Contract No.20093402110030).

## VI. Appendix

### VI.1 Appendix A: The relevant couplings

The Feynman rules for the coupling vertices in the LHT related to our work are listed in Table 4 [20, 40, 24, 41], where we denote  $P_{L,R} = \frac{1}{2}(1 \mp \gamma_5)$  and  $v = v_{SM}$ .

Vertex	Feynman rule	Vertex	Feynman rule
$W_H^{+\mu}(k_1)W_H^{-\nu}(k_2)A^\rho(k_3)$	$-ie[g^{\mu\nu}(k_1 - k_2)^\rho + g^{\nu\rho}(k_2 - k_3)^\mu + g^{\rho\mu}(k_3 - k_1)^\nu]$	$W_H^{+\nu}(k_1)W_H^{-\nu}(k_2)Z^\rho(k_3)$	$-ie\frac{c_w}{s_w}[g^{\mu\nu}(k_1 - k_2)^\rho + g^{\nu\rho}(k_2 - k_3)^\mu + g^{\rho\mu}(k_3 - k_1)^\nu]$
$W_{H\mu}^+\bar{U}_jD_{i-}(i = 1, 2, j = 1, 2, 3)$	$i\frac{g}{\sqrt{2}}\gamma_\mu P_L(V_{Hu})_{ij}$	$W_{H\mu}^-\bar{D}_jU_{i-}(i, j = 1, 2, 3)$	$i\frac{g}{\sqrt{2}}\gamma_\mu P_L(V_{Hd})_{ij}$
$W_{H\mu}^+\bar{t}D_{j-}(j = 1, 2, 3)$	$i\frac{g}{\sqrt{2}}\gamma_\mu c_L P_L(V_{Hu})_{j3}$	$hW_{H\mu}^+W_{H\nu}^-$	$-ie\frac{m_W}{s_w}g_{\mu\nu}$
$W_{H\mu}^-\bar{T}_+D_{j-}(j = 1, 2, 3)$	$i\frac{g}{\sqrt{2}}\gamma_\mu s_L P_L(V_{Hu})_{j3}$	$h\bar{T}_+T_+$	$i\frac{m_t c_\alpha s_\alpha}{f}$
$h\bar{U}_{i-}U_{i-}(i = 1, 2, 3)$	$i\frac{\sqrt{2}k_\nu v}{4f}$	$h\bar{t}t$	$-i\frac{m_t}{v}\left[1 - \left(\frac{3}{4} - c_\alpha^2 + c_\alpha^4\right)\frac{v^2}{f^2}\right]$
$Z_\mu\bar{U}_{i-}U_{i-}(i = 1, 2, 3)$	$i\frac{g}{c_w}\gamma_\mu\left(\frac{1}{2} - \frac{2}{3}s_w^2\right)$	$Z_\mu\bar{T}_-T_-$	$i\frac{g}{c_w}\gamma_\mu\left(-\frac{2}{3}s_w^2\right)$
$Z_\mu\bar{D}_{i-}D_{i-}(i = 1, 2, 3)$	$i\frac{g}{c_w}\gamma_\mu\left(-\frac{1}{2} + \frac{1}{3}s_w^2\right)$	$Z_\mu\bar{T}_+T_+$	$i\frac{g}{c_w}\gamma_\mu\left[\left(-\frac{2}{3}s_w^2 + \frac{s_\alpha^4 v^2}{f^2}\right)P_L - \frac{2}{3}s_w^2 P_R\right]$
$Z_\mu\bar{t}t$	$i\frac{g}{c_w}\gamma_\mu\left[\left(\frac{1}{2} - \frac{2}{3}s_w^2 - \frac{s_\alpha^4 v^2}{f^2}\right)P_L - \frac{2}{3}s_w^2 P_R\right]$	$A_{H\mu}\bar{U}_jU_{i-}(i, j = 1, 2)$	$i\left(-\frac{g c_H}{2} - \frac{g' s_H}{10}\right)\gamma_\mu P_L(V_{Hu})_{ij}$
$Z_{H\mu}\bar{U}_jU_{i-}(i, j = 1, 2)$	$i\left(\frac{g c_H}{2} - \frac{g' s_H}{10}\right)\gamma_\mu P_L(V_{Hu})_{ij}$	$A_{H\mu}\bar{D}_jD_{i-}(i, j = 1, 2, 3)$	$i\left(\frac{g s_H}{2} - \frac{g' c_H}{10}\right)\gamma_\mu P_L(V_{Hd})_{ij}$
$Z_{H\mu}\bar{D}_jD_{i-}(i, j = 1, 2, 3)$	$i\left(-\frac{g c_H}{2} - \frac{g' s_H}{10}\right)\gamma_\mu P_L(V_{Hd})_{ij}$	$A_{H\mu}\bar{t}t_-$	$i\left(-\frac{g s_H}{2} - \frac{g' c_H}{10}\right)c_L\gamma_\mu P_L(V_{Hu})_{33}$
$Z_{H\mu}\bar{t}t_-$	$i\left(\frac{g c_H}{2} - \frac{g' s_H}{10}\right)c_L\gamma_\mu P_L(V_{Hu})_{33}$	$G_\mu^a\bar{T}_\pm^a T_\pm^\beta$	$ig_s(T^a)_{\alpha\beta}\gamma_\mu$
$G_\mu^a\bar{q}_-^\alpha q_-^\beta$	$ig_s(T^a)_{\alpha\beta}\gamma_\mu$		

Table 4: The related LHT Feynman rules used in our calculations. There  $c_L = \sqrt{1 - s_\alpha^4 \frac{v^2}{f^2}}$ ,  $s_L = s_\alpha^2 \frac{v}{f}$ ,  $U_i = u, c, t$ ,  $D_i = d, s, b$ ,  $U_{i-} = u_-, c_-, t_-$  and  $D_{i-} = d_-, s_-, b_-$ .  $i$  and  $j$  are the generation indices.

### VI.2 Appendix B: Partial decay widths

The partial decay widths of  $T$ -odd up-type and down-type quarks can be generally expressed as

$$\begin{aligned}
\Gamma(U_{i-} \rightarrow W_H^+ D_j) &= \frac{g^2 |(V_{Hd})_{ij}|^2 m_{U_{i-}}^3}{64\pi m_{W_H}^2} \left[ \left(1 - \frac{m_{W_H}^2}{m_{U_{i-}}^2}\right) \left(1 + \frac{2m_{W_H}^2}{m_{U_{i-}}^2}\right) + \right. \\
&+ \left. \frac{m_{D_j}^2}{m_{U_{i-}}^4} \left(m_{D_j}^2 + m_{W_H}^2 - 2m_{U_{i-}}^2\right) \right] \left[ \left(1 - \left(\frac{m_{W_H} + m_{D_j}}{m_{U_{i-}}}\right)^2\right) \left(1 - \left(\frac{m_{W_H} - m_{D_j}}{m_{U_{i-}}}\right)^2\right) \right]^{\frac{1}{2}}, \\
&\hspace{15em} (i, j = 1, 2, 3), \\
\Gamma(U_{i-} \rightarrow Z_H U_j) &= \frac{2|(V_{Hu})_{ij}|^2 \left(\frac{g c_H}{2} - \frac{g' s_H}{10}\right)^2 m_{U_{i-}}^3}{64\pi m_{Z_H}^2} \left[ \left(1 - \frac{m_{Z_H}^2}{m_{U_{i-}}^2}\right) \left(1 + \frac{2m_{Z_H}^2}{m_{U_{i-}}^2}\right) + \right.
\end{aligned}$$

$$\begin{aligned}
& + \frac{m_{U_j}^2}{m_{U_{i-}}^4} \left( m_{U_j}^2 + m_{Z_H}^2 - 2m_{U_{i-}}^2 \right) \left[ \left( 1 - \left( \frac{m_{Z_H} + m_{U_j}}{m_{U_{i-}}} \right)^2 \right) \left( 1 - \left( \frac{m_{Z_H} - m_{U_j}}{m_{U_{i-}}} \right)^2 \right) \right]^{\frac{1}{2}}, \\
& \hspace{15em} (i, j = 1, 2), \\
\Gamma(U_{i-} \rightarrow A_H U_j) &= \frac{2|(V_{Hu})_{ij}|^2 \left( \frac{g_{sH}}{2} + \frac{g'_{sH}}{10} \right)^2 m_{U_{i-}}^3}{64\pi m_{A_H}^2} \left[ \left( 1 - \frac{m_{A_H}^2}{m_{U_{i-}}^2} \right) \left( 1 + \frac{2m_{A_H}^2}{m_{U_{i-}}^2} \right) + \right. \\
& + \left. \frac{m_{U_j}^2}{m_{U_{i-}}^4} \left( m_{U_j}^2 + m_{A_H}^2 - 2m_{U_{i-}}^2 \right) \right] \left[ \left( 1 - \left( \frac{m_{A_H} + m_{U_j}}{m_{U_{i-}}} \right)^2 \right) \left( 1 - \left( \frac{m_{A_H} - m_{U_j}}{m_{U_{i-}}} \right)^2 \right) \right]^{\frac{1}{2}}, \\
& \hspace{15em} (i, j = 1, 2), \\
\Gamma(t_- \rightarrow Z_H t) &= \frac{2|(V_{Hu})_{33}|^2 \left( \frac{g_{cH}}{2} - \frac{g'_{sH}}{10} \right)^2 c_L^2 m_{t_-}^3}{64\pi m_{Z_H}^2} \left[ \left( 1 - \frac{m_{Z_H}^2}{m_{t_-}^2} \right) \left( 1 + \frac{2m_{Z_H}^2}{m_{t_-}^2} \right) + \right. \\
& + \left. \frac{m_t^2}{m_{t_-}^4} \left( m_t^2 + m_{Z_H}^2 - 2m_{t_-}^2 \right) \right] \left[ \left( 1 - \left( \frac{m_{Z_H} + m_t}{m_{t_-}} \right)^2 \right) \left( 1 - \left( \frac{m_{Z_H} - m_t}{m_{t_-}} \right)^2 \right) \right]^{\frac{1}{2}}, \\
\Gamma(t_- \rightarrow A_H t) &= \frac{2|(V_{Hu})_{33}|^2 \left( \frac{g_{sH}}{2} + \frac{g'_{cH}}{10} \right)^2 c_L^2 m_{t_-}^3}{64\pi m_{A_H}^2} \left[ \left( 1 - \frac{m_{A_H}^2}{m_{t_-}^2} \right) \left( 1 + \frac{2m_{A_H}^2}{m_{t_-}^2} \right) + \right. \\
& + \left. \frac{m_t^2}{m_{t_-}^4} \left( m_t^2 + m_{A_H}^2 - 2m_{t_-}^2 \right) \right] \left[ \left( 1 - \left( \frac{m_{A_H} + m_t}{m_{t_-}} \right)^2 \right) \left( 1 - \left( \frac{m_{A_H} - m_t}{m_{t_-}} \right)^2 \right) \right]^{\frac{1}{2}}, \\
& \hspace{15em} (6.1)
\end{aligned}$$

$$\begin{aligned}
\Gamma(D_{i-} \rightarrow W_H^- U_j) &= \frac{g^2 |(V_{Hu})_{ij}|^2 m_{D_{i-}}^3}{64\pi m_{W_H}^2} \left[ \left( 1 - \frac{m_{W_H}^2}{m_{D_{i-}}^2} \right) \left( 1 + \frac{2m_{W_H}^2}{m_{D_{i-}}^2} \right) + \right. \\
& + \left. \frac{m_{U_j}^2}{m_{D_{i-}}^4} \left( m_{U_j}^2 + m_{W_H}^2 - 2m_{D_{i-}}^2 \right) \right] \left[ \left( 1 - \left( \frac{m_{W_H} + m_{U_j}}{m_{D_{i-}}} \right)^2 \right) \left( 1 - \left( \frac{m_{W_H} - m_{U_j}}{m_{D_{i-}}} \right)^2 \right) \right]^{\frac{1}{2}}, \\
& \hspace{15em} (i = 1, 2, j = 1, 2, 3), \\
\Gamma(b_- \rightarrow W_H^- t) &= \frac{g^2 |(V_{Hu})_{33}|^2 c_L^2 m_{b_-}^3}{64\pi m_{W_H}^2} \left[ \left( 1 - \frac{m_{W_H}^2}{m_{b_-}^2} \right) \left( 1 + \frac{2m_{W_H}^2}{m_{b_-}^2} \right) + \right. \\
& + \left. \frac{m_t^2}{m_{b_-}^4} \left( m_t^2 + m_{W_H}^2 - 2m_{b_-}^2 \right) \right] \left[ \left( 1 - \left( \frac{m_{W_H} + m_t}{m_{b_-}} \right)^2 \right) \left( 1 - \left( \frac{m_{W_H} - m_t}{m_{b_-}} \right)^2 \right) \right]^{\frac{1}{2}}, \\
\Gamma(D_{i-} \rightarrow Z_H D_j) &= \frac{2|(V_{Hd})_{ij}|^2 \left( \frac{g_{cH}}{2} + \frac{g'_{sH}}{10} \right)^2 m_{D_{i-}}^3}{64\pi m_{Z_H}^2} \left[ \left( 1 - \frac{m_{Z_H}^2}{m_{D_{i-}}^2} \right) \left( 1 + \frac{2m_{Z_H}^2}{m_{D_{i-}}^2} \right) + \right. \\
& + \left. \frac{m_{D_j}^2}{m_{D_{i-}}^4} \left( m_{D_j}^2 + m_{Z_H}^2 - 2m_{D_{i-}}^2 \right) \right] \left[ \left( 1 - \left( \frac{m_{Z_H} + m_{D_j}}{m_{D_{i-}}} \right)^2 \right) \left( 1 - \left( \frac{m_{Z_H} - m_{D_j}}{m_{D_{i-}}} \right)^2 \right) \right]^{\frac{1}{2}}, \\
& \hspace{15em} (i, j = 1, 2, 3),
\end{aligned}$$

$$\begin{aligned}
\Gamma(D_{i-} \rightarrow A_H D_j) &= \frac{2|(V_{Hd})_{ij}|^2 \left(\frac{g_{SH}}{2} - \frac{g'_{cH}}{10}\right)^2 m_{D_{i-}}^3}{64\pi m_{A_H}^2} \left[ \left(1 - \frac{m_{A_H}^2}{m_{D_{i-}}^2}\right) \left(1 + \frac{2m_{A_H}^2}{m_{D_{i-}}^2}\right) + \right. \\
&+ \left. \frac{m_{D_j}^2}{m_{D_{i-}}^4} (m_{D_j}^2 + m_{A_H}^2 - 2m_{D_{i-}}^2) \right] \left[ \left(1 - \left(\frac{m_{A_H} + m_{D_j}}{m_{D_{i-}}}\right)^2\right) \left(1 - \left(\frac{m_{A_H} - m_{D_j}}{m_{D_{i-}}}\right)^2\right) \right]^{\frac{1}{2}}. \\
&\hspace{15em} (i, j = 1, 2, 3),
\end{aligned} \tag{6.2}$$

The LO total decay width of the  $T$ -odd quark  $q_-$  can be obtained approximately by summing up all the LO partial decay widths of the main decay channels. In Eqs.(6.1) and (6.2),  $U_{i-} = u_-, c_-, t_-$ ,  $D_{i-} = d_-, s_-, b_-$ ,  $U_i = u, c, t$  and  $D_i = d, s, b$ .

## References

- [1] S. L. Glashow, Nucl. Phys. **22** (1961) 579; S. Weinberg, Phys. Rev. Lett. **19** (1967) 1264; A. Salam, Proc. 8th Nobel Symposium Stockholm 1968, ed. N. Svartholm (Almqvist and Wiksells, Stockholm 1968) p.367; H. D. Politzer, Phys. Rept. **14** (1974) 129.
- [2] P. W. Higgs, Phys. Lett. **12** (1964) 132, Phys. Rev. Lett. **13** (1964) 508, Phys. Rev. **145** (1966) 1156; F. Englert and R. Brout, Phys. Rev. Lett. **13** (1964) 321; G. S. Guralnik, C. R. Hagen and T. W. B. Kibble, Phys. Rev. Lett. **13** (1964) 585; T. W. B. Kibble, Phys. Rev. **155** (1967) 1554.
- [3] G.G. Ross, Grand Unified Theories (Addison-Wesley Publishing Company, Reading, MA, (1984); P. Langacker, Phys. Rep. **72** (1981) 185; H. Georgi, S.L Glashow, Phys. Rev. Lett. **32** (1974) 438; A.J. Buras, J. Ellis, M.K. Gaillard, D.V. Nanopoulos, Nucl. Phys. **B135**(1978) 66.
- [4] S. P. Martin, arXiv:hep-ph/9709356; M. E. Peskin, arXiv:0801.1928 [hep-ph]; K. A. Olive, arXiv:hep-ph/9911307; M. Drees, arXiv:hep-ph/9611409; H. E. Haber and G. L. Kane, Phys. Rept. **117** (1985) 75; H. P. Nilles, Phys. Rept. **110**, 1 (1984); A. Signer, J.Phys.**G36** (2009) 073002, arXiv:0905.4630 [hep-ph].
- [5] N. Arkani-Hamed, S. Dimopoulos, G. Dvali, Phys. Lett. **B429** (34): 263(1998), arXiv:hep-ph/9803315; N. Arkani-Hamed, S. Dimopoulos, G. Dvali, Phys. Rev. **D59** 086004(1999), arXiv:hep-ph/9807344; I. Antoniadis, N. Arkani-Hamed, S. Dimopoulos, G. Dvali, Phys. Lett. **B436** (34): 257(1998), arXiv:hep-ph/9804398; M. Shifman, Int. J. Mod. Phys. **A25** 199-225,2010, arXiv:0907.3074v2 [hep-ph].
- [6] R. N. Mohapatra and J. C. Pati, Phys. Rev. **D11** (1975), 566571; G. Senjanovic and R. N. Mohapatra; Phys. Rev. **D12** (1975), 1502; A. Adulpravitchai, M. Lindner, A. Merle, and R. N. Mohapatra, Phys. Lett. **B680** (2009) 476, arXiv/hep-ph:0908.0470.
- [7] L.Basso, S. Moretti, G.M. Pruna, Phys. Rev.**D83**(2011) 055014, arXiv:1011.2612v4 [hep-ph].
- [8] N. Arkani-Hamed, A. G. Cohen and H. Georgi, Phys. Lett. **B513** (2001) 232; M. Schmaltz and D. Tucker-Smith, Ann. Rev. Nucl. Part. Sci. **55** (2005) 229; M. Perelstein, Prog. Part. Nucl. Phys. **58** (2007) 247; and references therein.

- [9] Arkani-Hamed, A. G. Cohen, E. Katz, A. E. Nelson, T. Gregoire and J. G. Wacker, *JHEP* **08** (2002) 021.
- [10] N. Arkani-Hamed, A. G. Cohen, T. Gregoire, J. G. Wacker and A. G. Cohen, *JHEP* **08** (2002) 020.
- [11] I. Low, W. Skiba and D. Smith, *Phys. Rev.* **D66**, (2002) 072001.
- [12] C. Csaki, J. Hubisz, G. D. Kribs, P. Meade and J. Terning, *Phys. Rev.* **D67** (2003) 115002, [arXiv:hep-ph/0211124].
- [13] M. Schmaltz, *Nucl. Phys. Proc. Suppl.* **117** (2003) 40.
- [14] T. Gregoire and J. G. Wacker, *JHEP* **08** (2002) 019.
- [15] N. Arkani-Hamed, A. G. Cohen, E. Katz and A. E. Nelson, *JHEP* **07** (2002) 034.
- [16] ATLAS Collaboration, *Phys. Lett.* **B705** (2011) 18-46.
- [17] D. Olivito, for the ATLAS collaboration, Conference proceedings for the Meeting of the Division of Particles and Fields of the American Physical Society (DPF), 2011, arXiv:1109.0934.
- [18] I. Low, *JHEP* **0410** (2004) 067.
- [19] R. Barbieri and A. Strumia, IFUP-TH/2000-22 and SNS-PH/00-12, [arXiv:hep-ph/0007265].
- [20] J. Hubisz and P. Meade, *Phys. Rev.* **D71** (2005) 035016.
- [21] J. Hubisz, P. Meade, A. Noble and M. Perelstein, *JHEP* **01** (2006) 135.
- [22] H.-C. Cheng and I. Low, *JHEP* **09** (2003) 051; *JHEP* **08** (2004) 061.
- [23] A. Birkedal, A. Noble, M. Perelstein and A. Spray, *Phys. Rev.* **D74** (2006) 035002; M. Asano, S. Matsumoto, N. Okada, and Y. Okada, *Phys. Rev.* **D75** (2007) 063506.
- [24] A. Belyaev, C. -R. Chen, K. Tobe and C. -P. Yuan, *Phys. Rev.* **D74**, (2006) 115020.
- [25] A. Belyaev, C. -R. Chen, K. Tobe and C. -P. Yuan, in Proceedings of Monte Carlo Tools for Beyond the Standard Model Physics, Fermilab, 2006, given by A. Belyaev,

- <http://theory.fnal.gov/mc4bsm/agenda.html>; in Proceedings of Osaka University, 2006, Osaka, given by C. -P. Yuan, <http://www-het.phys.sci.osaka-u.ac.jp/seminar/seminar/seminar.html>; in Proceedings of the Summer Institute on Collider Phenomenology, National Tsing Hua University, Taiwan, 2006, given by K. Tobe, <http://charm.phys.nthu.edu.tw/hep/summer2006/>; in Proceedings of ICHEP'06, Moscow, 2006, given by A. Belyaev, [http://ichep06.jinr.ru/reports/116\\_11s1\\_10p20\\_belyaev.pdf](http://ichep06.jinr.ru/reports/116_11s1_10p20_belyaev.pdf).
- [26] C.-S. Chen, K. Cheung and T. -C. Yuan, Phys. Lett. **B644** (2007) 158.
- [27] R.-Y. Zhang, H. Yan, W.-G. Ma, S.-M. Wang, L. Guo and L. Han, Phys. Rev. **D85** (2012)015017.
- [28] Qing-Hong Cao and Chuan-Ren Chen, Phys. Rev. **D76** (2007) 075007.
- [29] J. Hubisz, P. Meade, A. Noble and M. Perelstein, JHEP **0601**, 135 (2006), arXiv:hep-ph/0506042.
- [30] T.Hahn, Comput.Phys.Commun. **140** (2001) 418.
- [31] T.Hahn, M.Perez-Victoria, Comput.Phys.Commun. **118** (1999) 153.
- [32] B. W. Harris and J. F. Owens, Phys. Rev. **D65** (2002) 094032.
- [33] T. Kinoshita, J. Math. Phys. **3** (1962) 650; T. D. Lee and M. Nauenberg, Phys. Rev. **133** (1964) B1549.
- [34] W. Beenakker, R. Höpker, M. Spira and P. M. Zerwas, Nucl. Phys. **B492** (1997) 51; W. Beenakker, M. Klasen, M. Krämer, T. Plehn, M. Spira and P. M. Zerwas, Phys. Rev. Lett. **83** (1999) 3780; <http://www.thphys.uni-heidelberg.de/~plehn/index.php?show=prospino>.
- [35] T. Plehn and C. Weydert, PoS **CHARGED2010** (2010) 026, [arXiv:1012.3761]; T. Binoth, D. Goncalves-Netto, D. Lopez-Val, K. Mawatari, T. Plehn and I. Wigmore, Phys. Rev. D **84** (2011) 075005, [arXiv:1108.1250].
- [36] M. Blanke, A. J. Buras, A. Poschenrieder, S. Recksiegel, C. Tarantino, S. Uhlig and A. Weiler JHEP **01** (2007) 066.
- [37] K. Nakamura, *et al.*, J. Phys. **G37** (2010) 075021.

- [38] J. Pumplin, D. R. Stump, J. Huston, H. -L. Lai, P. Nadolsky and W. -K. Tung, JHEP **07** (2002) 012; D. Stump, J. Huston, J. Pumplin, W. -K. Tung, H. -L. Lai, S. Kuhlmann and J. F. Owens, JHEP **10** (2003) 046.
- [39] S. Dittmaier, Nucl. Phys. **B 565** 69(2000), arXiv:hep-ph/9904440; M. Roth, PhD thesis, ETH Zürich No. 13363 (1999), arXiv:hep-ph/0008033.
- [40] T. Han, H.E. Logan, B. McElrath, and L.T. Wang, Phys. Rev. **D67**,095004(2003).
- [41] K. Pan, R.-Y. Zhang, W.-G. Ma, H. Sun, L. Han, and Y. Jiang, Phys. Rev. **D76**,015012(2007).